Model falsification from a Bayesian viewpoint with applications to parameter inference and model selection of dynamical systems

Agnimitra Dasgupta[1] and Erik A. Johnson, Member, ASCE[2]

[1]Sonny Astani Department of Civil and Environmental Engineering, Viterbi School of Engineering, University of Southern California, 3620 S. Vermont Avenue, KAP 210, Los Angeles, CA 90089-2531. E-mail: adasgupt@usc.edu.

[2]Sonny Astani Department of Civil and Environmental Engineering, Viterbi School of Engineering, University of Southern California, 3620 S. Vermont Avenue, KAP 210, Los Angeles, CA 90089-2531. E-mail: JohnsonE@usc.edu.

ABSTRACT

The objective of this work is to provide a Bayesian re-interpretation to model falsification. We show that model falsification can be viewed as an approximate Bayesian computation (ABC) approach when hypotheses (models) are sampled from a prior. To achieve this, we recast model falsifiers as discrepancy metrics and density kernels such that they may be adopted within ABC and generalized ABC (GABC) methods. We call the resulting frameworks model falsified ABC and GABC, respectively. Moreover, as a result of our reinterpretation, the set of unfalsified models can be shown to be realizations of an approximate posterior. We consider both error and likelihood domain model falsification in our exposition. Model falsified (G)ABC is used to tackle two practical inverse problems albeit with synthetic measurements. The first type of problem concerns parameter estimation and includes applications of ABC to the inference of a statistical model where the likelihood can be difficult to compute, and the identification of a cubic-quintic dynamical system. The second type of example involves model selection for the base isolation system of a four degree-of-freedom base isolated structure. The performance of model falsified

ABC and GABC are compared with Bayesian inference. The results show that model falsified (G)ABC can be used to solve inverse problems in a computationally efficient manner. The results are also used to compare the various falsifiers in their capability of approximating the posterior and some of its important statistics. Further, we show that model falsifier based density kernels can be used in kernel regression to infer unknown model parameters and compute structural responses under epistemic uncertainty.

INTRODUCTION

Model falsification is a simulation-based inference approach that is based on the Popperian notion of falsifiability: any hypothesis unable to predict observations must be rejected. The basic idea behind model falsification is to find useful models by comparing simulations from each model against the available measurements. There are two different approaches for model falsification — error domain and likelihood domain model falsification. The error domain model falsification, which is a likelihood-free approach, was developed by Goulet et al. (2010). In error domain model falsification, models are falsified if the difference between the predictions and the measurements exceed bounds that are derived after accounting for uncertainty arising from different sources. Error domain model falsification has been used for system identification (Goulet and Smith 2013b; Pasquier and Smith 2015) and in many other applications (Goulet et al. 2013; Goulet and Smith 2013a; Moser et al. 2018; Pai et al. 2018). Likelihood domain model falsification was proposed by De et al. (2018) and draws on ideas from the generalized likelihood uncertainty estimation (GLUE) methods (Beven 1993; Beven and Freer 2001; Beven 2011). In the likelihood domain, models are falsified based on the likelihood value of their prediction errors. It must be stressed here that the likelihood values may even be computed based on an assumed probability density for the prediction errors. Regardless of the falsification methodology adopted, model falsification appears to be a frequentist approach to inference since hypothesis testing lies at its core. Every model (or hypothesis) is rejected or accepted based on its merit (the capability to predict what has been observed) as controlled via a target identification probability. The unfalsified models form a candidate set (Goulet and Smith 2013b; De et al. 2018) that can be considered to comprise the solutions to the inverse problem at hand.

The debate on differences and similarities between Bayesian and frequentist approaches to inference has been on-going; see, for instance, (Freedman 1997; Freedman and Stark 2003; Stark and Tenorio 2010; Milne 1995; Rosenkrantz 1977). In fact, error domain model falsification is similar to Bayesian inference with a modified likelihood (Pai and Smith 2017; Pai et al. 2018). Similarly, Sadegh and Vrugt (2013) have discussed similarities between the GLUE approach and ABC. Our work was motivated by these suggestions of similarity between model falsification, and similar inference approaches, and Bayesian inference. However, one difference that we need to note at the outset is the necessity of defining a prior. Consider the inference of a parameter θ. Bayesian inference requires that a prior probability density $\pi(\theta)$ be specified (Evans and Stark 2002); the prior represents subjective knowledge of the various hypotheses. On the other hand, model falsification does not require that a prior probability density be specified: specifying $\theta \in \Omega$, such that one can sample from Ω, may be sufficient for model falsification. However, in practice, models are conveniently sampled from a prior density and subsequently subject to falsification (De et al. 2018). This has, in particular, enabled the application of falsification to high-dimensional problems involving multiple random variables. The specification of a prior has also been a convenient way of introducing subjective information, which is at the very least a non-informative (a uniform prior over Ω), within model falsification. This approach of sampling models from a prior and subjecting them to model falsification, as we shall reveal, resembles approximate Bayesian computation (ABC) where the falsifier (defined later) plays the role of a discrepancy metric.

ABC is also a simulation-based inference method commonly used when the likelihood function is either unavailable or difficult to compute. Beaumont et al. (2002) is credited with coining the term *approximate Bayesian computation*, although the ideas behind ABC predates them (Rubin 1984; Tavaré et al. 1997; Pritchard et al. 1999). Briefly, ABC methods sidestep the likelihood function by simulating predictions from different parameters of a model class, and accepting them if, according to some discrepancy metric, simulations match the observed data. ABC methods have been applied in civil engineering for model selection and/or parameter estimation of dynamical systems (Toni et al. 2009; Abdessalem et al. 2018; Abdessalem et al. 2019; Chiachio et al. 2014; Vakilzadeh et al. 2017; Barros et al. 2022), estimating the parameters of degradation processes (Hazra et al. 2020; Hazra and Pandey 2021), damage detection (Fang et al. 2019), and the calibration of hydrological models (Vrugt and Sadegh 2013). A further class of methods known as generalized ABC (GABC), first proposed by Wilkinson (2014), uses density kernels, instead of discrepancy metrics, to assess the similarity of model predictions and measurements.

We argue that model falsification is nothing but ABC by showing that the methodology of model falsification resembles rejection sampling based ABC, and refer to it as *model falsified ABC*. Incorporated within model falsified ABC is a model falsifier acting as a discrepancy metric. Building on our preliminary study (Dasgupta and Johnson 2022), our presentation is fairly general as we show this for four different types of model falsifiers that are representative of the wide gamut of falsifiers; other falsifiers not covered herein can also be easily used. We also show that model falsifiers can be recast as density kernels, and introduce model falsified GABC that makes use of these kernels. Further, we show that the set of unfalsified models are realizations drawn from the approximate posterior distribution, formally providing a Bayesian perspective on model falsification. Moreover, the ratio of unfalsified models from different model classes can be shown to approximate the posterior probability of the respective model classes. The re-purposing of falsifiers as kernels further allows for their use in kernel regression (Wasserman 2006). We show that kernel regression can be performed using density kernels based on model falsifiers while exploiting Nadaraya-Watson estimates (Wasserman 2006; Blum 2010). We use model falsification based kernel regression for non-parametric inference of unknown parameters, and response prediction when the true model class is unknown.

The remainder of the paper is organized as follows. In Section 2, Bayesian inference and ABC are reviewed very briefly, and a background on model falsification is provided in modest detail. Various falsifiers are also introduced in Section 2. In Section 3, we recast falsifiers as discrepancy metrics and density kernels, and discuss some of their properties. In Section 4, we make the formal connection between model falsification and ABC and introduce model falsified ABC and GABC;

for brevity, we refer to these two approaches together as model falsified (G)ABC. Next, model falsified (G)ABC is applied to two types of inverse problems in Sections 5 and 6. In Section 5, model falsified (G)ABC is applied to parameter inference problems; two examples are considered — a toy example and a dynamical system. In Section 6, the behavior of a base isolated building modeled as a four degree-of-freedom system is inferred using model falsified (G)ABC. In Section 7, kernel regression using falsifiers is introduced and applied to parameter estimation and response prediction. We discuss some implications of this work and future research directions in Section 8, and conclude the paper in Section 9.

BACKGROUND ON DIFFERENT APPROACHES FOR INVERSE PROBLEMS INVOLVING PARAMETER ESTIMATION

The goal of any parameter estimation problem is to infer the unknown parameter $\boldsymbol{\theta} \in \boldsymbol{\Theta} \subseteq \mathbb{R}^{N_\theta}$ of a parameterized model class $\mathcal{M}$ using noisy measurements $\mathbf{d} \in \mathfrak{D} \subseteq \mathbb{R}^{N_m}$. A realization of $\boldsymbol{\theta}$ is often called a *model*. Corresponding to the measurements $\mathbf{d}$, a prediction $\mathbf{y} \in \mathfrak{D}$ from the model $\boldsymbol{\theta}$ is a realization of the random variable $\boldsymbol{y}$ drawn from the distribution $\pi(\boldsymbol{y}|\boldsymbol{\theta}, \mathcal{M})$.

Bayesian Inference

In Bayesian inference (BI), prior belief (or knowledge) about $\boldsymbol{\theta}$ is updated using the observations $\mathbf{d}$ to obtain the posterior belief about $\boldsymbol{\theta}$. The prior probability density function (pdf), noise model and posterior pdf are denoted as $\pi(\boldsymbol{\theta}|\mathcal{M})$, $\pi(\mathbf{d}|\boldsymbol{y}, \boldsymbol{\theta}, \mathcal{M})$ and $\pi(\boldsymbol{\theta}|\mathbf{d})$, respectively. Further, let

$$\ell(\mathbf{d}|\boldsymbol{\theta}, \mathcal{M}) = \int_{\mathfrak{D}} \pi(\mathbf{d}|\boldsymbol{y}, \boldsymbol{\theta}, \mathcal{M})\pi(\boldsymbol{y}|\boldsymbol{\theta}, \mathcal{M})\, \mathrm{d}\boldsymbol{y} \tag{1}$$

be the likelihood function. Bayes' theorem tells us that $\pi(\boldsymbol{\theta}|\mathbf{d}, \mathcal{M}) \propto \ell(\mathbf{d}|\boldsymbol{\theta}, \mathcal{M})\pi(\boldsymbol{\theta}|\mathcal{M})$. Thus, Bayes' theorem helps characterize all possible solutions to the inverse problem using the posterior pdf $\pi(\boldsymbol{\theta}|\mathbf{d}, \mathcal{M})$, which also reflects the relative plausibility of different solutions. Herein, the conditional dependence on model class $\mathcal{M}$ is suppressed for notational simplicity.

Approximate Bayesian Computation

The likelihood function ℓ may be unknown or intractable, which can make evaluations of the posterior pdf challenging. ABC methods were developed to overcome this difficulty. The basic idea is to evaluate the joint posterior $\pi(\boldsymbol{\theta}, \boldsymbol{y}|\mathbf{d})$ and then marginalize over $\boldsymbol{y}$. Using Bayes' theorem again,

$$\pi(\boldsymbol{\theta}, \boldsymbol{y}|\mathbf{d}) \propto \pi(\mathbf{d}|\boldsymbol{\theta}, \boldsymbol{y})\pi(\boldsymbol{y}|\boldsymbol{\theta})\pi(\boldsymbol{\theta}), \tag{2}$$

from which it follows that $\pi(\boldsymbol{\theta}|\mathbf{d}) = \int_{\mathfrak{D}} \pi(\boldsymbol{\theta}, \boldsymbol{y}|\mathbf{d})\, \mathrm{d}\boldsymbol{y}$. Setting $\pi(\mathbf{d}|\boldsymbol{\theta}, \boldsymbol{y}) = \mathcal{I}_{\mathcal{A}_{\mathbf{d}}}(\boldsymbol{y})$, where $\mathcal{I}_B$ is the indicator function of the set B and $\mathcal{A}_{\mathbf{d}} = \{\boldsymbol{y} \in \mathfrak{D} | \boldsymbol{y} = \mathbf{d}\}$, yields the posterior pdf $\pi(\boldsymbol{\theta}|\mathbf{d})$. However, the criteria $\boldsymbol{y} = \mathbf{d}$ is infeasible in a continuous setting. ABC methods circumvent this by using $\pi(\mathbf{d}|\boldsymbol{\theta}, \boldsymbol{y}) = \mathcal{I}_{\mathcal{A}_{\kappa,\mathbf{d}}}(\boldsymbol{y})$, instead of $\mathcal{I}_{\mathcal{A}_{\mathbf{d}}}(\boldsymbol{y})$, where κ is now a tolerance parameter or threshold, and

$$\mathcal{A}_{\kappa,\mathbf{d}}(\boldsymbol{y}) = \{\boldsymbol{y} \in \mathfrak{D} | \rho(\boldsymbol{y}, \mathbf{d}) \leq \kappa\}\,. \tag{3}$$

The function $\rho(\cdot,\cdot)$ is a metric for the discrepancy or degree of dissimilarity between model predictions $\boldsymbol{y}$ and measurements $\mathbf{d}$, and usually satisfies the property that $\rho(\boldsymbol{y}, \mathbf{d}) \to 0$ as $\boldsymbol{y} \to \mathbf{d}$. Eq. (3) leads to the joint pdf

$$\pi_{\mathrm{ABC}}(\boldsymbol{\theta}, \boldsymbol{y}|\mathbf{d}) \propto \mathcal{I}_{\mathcal{A}_{\kappa,\mathbf{d}}}(\boldsymbol{y})\pi(\boldsymbol{y}|\boldsymbol{\theta})\pi(\boldsymbol{\theta}) \tag{4}$$

which, after marginalization, ultimately yields an approximate posterior pdf

$$\pi_{\mathrm{ABC}}(\boldsymbol{\theta}|\mathbf{d}) \propto \pi(\boldsymbol{\theta}) \int_{\mathfrak{D}} \pi(\boldsymbol{y}|\boldsymbol{\theta})\, \mathcal{I}_{\mathcal{A}_{\kappa,\mathbf{d}}}(\boldsymbol{y})\, \mathrm{d}\boldsymbol{y} = P(\boldsymbol{y} \in \mathcal{A}_{\kappa,\mathbf{d}})\, \pi(\boldsymbol{\theta}). \tag{5}$$

Samples can be drawn from the approximate posterior pdf $\pi_{\mathrm{ABC}}(\boldsymbol{\theta}, \boldsymbol{y}|\mathbf{d})$ using the likelihood free rejection sampler described in Algorithm 1 (Sisson et al. 2018, Chapter 1) in Appendix I, and the marginalization of Eq. (5) can be performed by retaining only the $\boldsymbol{\theta}$ components of the generated samples. Note that $\pi_{\mathrm{ABC}}(\boldsymbol{\theta}|\mathbf{d})$ and $\pi(\boldsymbol{\theta}|\mathbf{d})$ are one and the same when $\kappa = 0$, meaning that the marginal distribution of the parameter $\boldsymbol{\theta}$ in samples drawn using Algorithm 1 with $\kappa = 0$ is the true posterior pdf $\pi(\boldsymbol{\theta}|\mathbf{d})$.

Accept/reject conditions like Eq. (3) do not utilize the degree of similarity between model predictions and measurements. With the view of utilizing that information, Wilkinson (2014) proposed GABC, where the indicator function $\mathcal{I}_{\mathcal{A}_{\kappa,\mathbf{d}}}(\boldsymbol{y})$ is replaced by a density kernel $k(\boldsymbol{y},\mathbf{d})$. The resultant joint posterior pdf is given as $\pi_{\mathrm{ABC}}(\boldsymbol{\theta},\boldsymbol{y}|\mathbf{d}) \propto k(\boldsymbol{y},\mathbf{d})\pi(\boldsymbol{y}|\boldsymbol{\theta})\pi(\boldsymbol{\theta})$, and the approximate posterior pdf is

$$\pi_{\mathrm{ABC}}(\boldsymbol{\theta}|\mathbf{d}) \propto \underbrace{\left\{\int_{\mathfrak{D}} k(\boldsymbol{y},\mathbf{d})\pi(\boldsymbol{y}|\boldsymbol{\theta})\ \mathrm{d}\boldsymbol{y}\right\}}_{\ell_{\mathrm{ABC}}(\mathbf{d}|\boldsymbol{\theta})}\pi(\boldsymbol{\theta}). \tag{6}$$

Let b be the bandwidth of the kernel k; as the bandwidth b of the kernel k approaches zero, k starts to resemble a Dirac-delta function; i.e., $k(\boldsymbol{y},\mathbf{d}) \to \delta_{\mathbf{d}}(\boldsymbol{y})$ as $b \to 0$, where $\delta_{\mathbf{d}}(\cdot)$ is the Dirac delta function centered around $\mathbf{d}$. As a result, $\pi_{\mathrm{ABC}}(\boldsymbol{\theta}|\mathbf{d}) \to \pi(\boldsymbol{\theta}|\mathbf{d})$ as $b \to 0$. The rejection ABC method of Algorithm 1 is a special case of the GABC method wherein a uniform kernel is used (Sisson et al. 2018). The GABC approach can also be considered Bayesian inference using the *approximate* likelihood ℓ_{ABC}. Realizations can be drawn from the approximate posterior using rejection sampling; see Algorithm 2 in Appendix I (Wilkinson 2013).

Model Falsification

Model falsification compares the model predictions to the observations $\mathbf{d}$ and accepts or rejects models, with all accepted (or unfalsified) models considered to be candidates for the solution to the inverse problem. The decision to falsify or unfalsify a model is made using a model falsifier function, denoted herein as f. Therefore, falsifiers are natural candidates for quantifying the degree of similarity between model predictions and measurements. A prediction $\mathbf{y}$ from a model $\boldsymbol{\theta}$ is unfalsified by f when

$$f(\mathbf{y},\mathbf{d}) \leq \kappa_{\phi}, \tag{7}$$

where the falsifier f and the threshold κ_{ϕ} depend on the model falsification approach and error control criteria adopted to falsify models, and the latter depends on the target identification probability ϕ. We consider two model falsification approaches: error domain and likelihood domain model falsification and use the subscripts E and L, respectively, to denote the respective falsifiers and their corresponding thresholds. Error control criteria that have been used for model falsification include the family wise error rate (FWER) and the false discovery rate (FDR); as the FWER is usually controlled using the Šidák correction (Abdi 2007), while the FDR is controlled using the Benjamini-Hochberg (BH) procedure (Benjamini and Hochberg 1995), we will use the subscripts S and B to denote Šidák and BH corrections, respectively. Thus, four subscripts on f and κ are used to denote the resulting cases: ES, EB, LS and LB. Irrespective of the falsification approach adopted, the model falsifier f is also a function of the error residual vector $\boldsymbol{\epsilon} = \mathbf{y} - \mathbf{d}$, which is the difference between model predictions and observations. Therefore, model falsifiers $f_{(\cdot)}$ can also be expressed as a function of $\boldsymbol{\epsilon}$; i.e., $f_{(\cdot)}(\mathbf{y}, \mathbf{d}) \equiv f_{(\cdot)}(\mathbf{y} - \mathbf{d}) \equiv f_{(\cdot)}(\boldsymbol{\epsilon})$.

For model falsification, the pdf of the components of the error residuals must be specified. Let $\epsilon_i = y_i - d_i$ be the i^{th} component of the error residual vector $\boldsymbol{\epsilon}$, and $\pi_{E_i}(e_i)$ be the pdf associated with ϵ_i, where E_i is the random variable corresponding to ϵ_i and e_i is the value ϵ_i assumes. The $\pi_{E_i}(e_i)$ are generally chosen based on the measurement process. Moreover, the target identification probability ϕ also must be chosen *a priori* and directly controls the type I and type II errors made by the falsifiers (De et al. 2018).

Error domain model falsification

In error domain model falsification, the model falsifier $f_{\mathrm{E}(\cdot)}$ — where $(\cdot)$ denotes one of the error control criteria — can be expressed as the composition of three functions; i.e., $f_{\mathrm{E}(\cdot)}(\mathbf{y}, \mathbf{d}) = f_3\left(f_{2,(\cdot)}\left(f_1(\mathbf{y}, \mathbf{d})\right)\right)$. First, the i^{th} component of $\mathbf{p} = f_1(\mathbf{y}, \mathbf{d})$ is computed using

$$p_i = 2 \min \left\{ \int_{-\infty}^{\epsilon_i} \pi_{E_i}(e_i) \mathrm{d}e_i \, , \, \int_{\epsilon_i}^{\infty} \pi_{E_i}(e_i) \mathrm{d}e_i \right\}. \tag{8}$$

$\mathbf{p}$ is the vector of p-values corresponding to the prediction $\mathbf{y}$. Second, $\tilde{\mathbf{p}} = f_{2,(\cdot)}(\mathbf{p})$ orders the p-values ($p^{(1)} \equiv p_{j_1} \leq p^{(2)} \equiv p_{j_2} \leq \ldots$, where $j_i \in \{1, 2, \ldots, N_m\}$ and $j_i \neq j_k$ for $i \neq k$) and scales them as $\tilde{p}_i = r_{i,(\cdot)} p^{(i)}$. The scaling factors r_i depend on the error control criteria used. Third, $f_3(\tilde{\mathbf{p}}) = 1 - \min_{i=1,\ldots,N_m} \tilde{p}_i$. The scaling factors and the thresholds for different model falsifiers in the error domain with different error control criteria are provided in Table 1.

Likelihood domain model falsification

Despite its name, likelihood domain model falsification does not require access to the true likelihood function necessary for Bayesian inference. Instead, models are falsified directly based on the likelihood of observing $\boldsymbol{\epsilon}$ as computed using the $\pi_{E_i}(e_i)$. The falsifier $f_{\mathrm{L}(\cdot)}$ is defined as,

$$f_{\mathrm{L}(\cdot)} = 1 - c_{(\cdot)} \prod_{i=1}^{N_m} \pi_{E_i}(\epsilon_i) \tag{9}$$

where $c_{(\cdot)}$ is a constant that is defined later. In the likelihood domain model falsification approach, $\kappa_{\mathrm{L}(\cdot),\phi}$ is an implicit function of ϕ and can be chosen based on bounds for the residual errors ϵ_i. Given a significance level α_i for the i^{th} error residue ϵ_i, upper and lower error bounds $\underline{\epsilon}_i$ and $\bar{\epsilon}_i$ can be computed from the following equation:

$$\frac{\alpha_i}{2} = \int_{-\infty}^{\underline{\epsilon}_i} \pi_{E_i}(e_i)\mathrm{d}e_i = \int_{\bar{\epsilon}_i}^{\infty} \pi_{E_i}(e_i)\mathrm{d}e_i. \tag{10}$$

The significance level α_i depends on the error control criteria and correction being used; see Table 1. Now, the threshold in the likelihood domain can be chosen as follows,

$$\kappa_{\mathrm{L}(\cdot),\phi} = 1 - c_{(\cdot),\phi} \prod_{i=1}^{N_m} \min_{\underline{\epsilon}_i \le e_i \le \bar{\epsilon}_i} \pi_{E_i}(e_i). \tag{11}$$

In Eqs. (9) and (11), $c_{(\cdot),\phi}^{-1} = \prod_{i=1}^{N_m} \max_{\underline{\epsilon}_i \le e_i \le \bar{\epsilon}_i} \pi_{E_i}(e_i)$ is the normalizing factor that also depends on the error control criteria being used. However, simplifying Eqs. (7), (9) and (11) results in

$$-\prod_{i=1}^{N_m} \pi_{E_i}(\epsilon_i) \le -\prod_{i=1}^{N_m} \min_{\underline{\epsilon}_i \le e_i \le \bar{\epsilon}_i} \pi_{E_i}(e_i), \tag{12}$$

where the left-hand-side of the inequality does not depend on the error control criteria. Thus, f_{LS} and f_{LB} will be effectively the same when implemented as Eq. (12).

RECASTING MODEL FALSIFIERS

In this section, we recast the model falsifiers first as discrepancy metrics and then as kernels. At this point, we make two practical assumptions about the marginal pdfs $\pi_{E_i}(e_i)$:

Assumption 1: $\mathbb{E}[E_i] = 0\ \forall i = 1, \ldots, N_m$; i.e., the residual errors are zero mean distributed;

Assumption 2: $\pi_{E_i}(e_i)$ is symmetric about the mean.

Assumption 1 can be made without any loss in generality. Assumption 2 is stronger and places a restriction on the type of distributions that can be used to statistically describe the error residuals. Assumption 2 enforces the condition that the mean and median coincide. Both assumptions are practically motivated, and are satisfied, for example, when the residues are zero-mean Gaussian distributed (a popular choice if arguments based on the principal of maximum entropy are used) or zero-mean Laplace distributed (when heavier tails are necessary).

As discrepancy metrics

In Eq. (7), model falsifiers have already been posed as discrepancy metrics, similar to ABC's Eq. (3). Additionally, due to the assumptions made above, all three falsifiers exhibit the following two important properties:

1. $f_{(\cdot)} = 0$ when $\mathbf{y} = \mathbf{d}$; i.e., the functions assume the minimum value of zero when the predictions match the measurements.

2. The falsifiers are non-decreasing functions of the error residual (some norm of $\boldsymbol{\epsilon}$ to be more precise). For example, in the one dimensional case, $f_{(\cdot)}$ is a non-decreasing function of $|\epsilon|$.

Thus, model falsifiers are natural candidates for measures of discrepancy between predictions $\mathbf{y}$ and data $\mathbf{d}$.

Figs. 1 and 2 show plots of the different falsifiers in one and two dimensions, respectively, where the error residuals are assumed to be independent standard normal variables. From Fig. 1, it can be seen that f_{ES} and f_{EB} are one and the same, but different from $f_{\text{L}(\cdot)}$. However, the functions are all different from each other in higher dimensions, as shown in Fig. 2. Also note that, $f_{\text{EB}} = 0$ not only at $(0, 0)$, but also along both coordinate axes. For example, for standard normal distributed error residues, any model $\boldsymbol{\theta}$ with error residuals $\epsilon_1 = 1$ and $|\epsilon_2| \leq 0.6745$ (or vice versa) will also result in $f_{\text{EB}} = 0$. However, both f_{ES} and $f_{\text{L}(\cdot)}$ are zeros if and only if $\mathbf{y} = \mathbf{d}$.

For the same value of the target identification probability, and independent standard normal distributed error resdiuals in two-dimensions, a comparison between the various falsifiers is shown in Fig. SM1 that can be found in Section SM1 of the Supplemental Material (described in Appendix IV) and also in (Dasgupta 2023). Falsifiers employing the Šidák correction are more conservative compared to falsifiers based on FDR control because the BH correction causes more models to be falsified at the same value of ϕ (De et al. 2018). Similarly, likelihood domain falsifiers are more conservative compared to their error domain counterparts (De et al. 2018).

As kernels

Model falsifiers can also be converted into density kernels. For a specified value of ϕ, error control criterion and model falsification method, let $k_{(\cdot)}$ be the kernel corresponding to the falsifier $f_{(\cdot)}$. We define $k_{\text{E}(\cdot)}$ as

$$k_{\text{E}(\cdot)}(\mathbf{y}, \mathbf{d}) = \begin{cases} \frac{1 - f_{\text{E}(\cdot)}(\mathbf{y}, \mathbf{d})}{V_{\text{E}(\cdot)}} & \text{if } f_{\text{E}(\cdot)}(\mathbf{y}, \mathbf{d}) \leq \kappa_{\text{E}(\cdot),\phi} \\ 0 & \text{otherwise,} \end{cases} \tag{13}$$

and $k_{\text{L}(\cdot)}$ as

$$k_{\text{L}(\cdot)}(\mathbf{y}, \mathbf{d}) = \frac{1 - f_{\text{L}(\cdot)}(\mathbf{y}, \mathbf{d})}{V_{\text{L}(\cdot)}}, \tag{14}$$

where $V_{(\cdot)}$ is a kernel specific constant which ensures that $\int k_{(\cdot)}(\boldsymbol{y}, \mathbf{d})\, \mathrm{d}\boldsymbol{y} = 1$, but $V_{(\cdot)}$ need not be computed for the purposes of numerical implementation. From Eq. (13), $k_{\text{E}(\cdot)}$ evaluates to zero if the model $\boldsymbol{\theta}$ is to be falsified based on the prediction $\mathbf{y}$. This means that kernels of type $k_{\text{E}(\cdot)}$ have a compact support. The kernels of type $k_{\text{L}(\cdot)}$ do need to be assigned a compact support, although a compact support can be assigned in a manner very similar to Eq. (13). Effectively, $k_{\text{LS}} = k_{\text{LB}}$ (the constant $c_{(\cdot),\phi}$ gets absorbed into $V_{\text{L}(\cdot)}$, and $V_{\text{LS}} = V_{\text{LB}}$), and we use k_{L} to commonly denote them. The reason we refrain from assigning the compact support will become clear in Section 4.

In one dimension, the kernels k_{ES} (which is equal to k_{EB} in the one dimensional case) and $k_{\mathrm{L}(\cdot)}$ are shown in Fig. 3. Fig. 4 shows plots of the different kernels in two dimensions where the error residuals are again assumed to be standard normal distributed. In both plots, $\phi = 0.90$ is chosen to assign compact support to the kernels. For kernels with compact support, the bandwidth along the i^{th} dimension is half the size of the interval over which $k_{(\cdot)} \neq 0$. Thus, the bandwidths of the kernels in this case implicitly depend on the marginal distributions of the error residuals, and the target identification probability ϕ. The bandwidth will reduce if ϕ is reduced and/or the assumed variance in the residual errors is reduced.

Validity of the kernels

Let $k'_{\mathrm{E}(\cdot)}(\mathbf{y}, \mathbf{d}) = \left\{1 - f_{\mathrm{E}(\cdot)(\mathbf{y},\mathbf{d})}\right\} \mathbb{I}\left[f_{\mathrm{E}(\cdot)}(\mathbf{y}, \mathbf{d}) \leq \kappa_{\mathrm{E}(\cdot),\phi}\right] = k_{\mathrm{E}(\cdot)} V_{\mathrm{E}(\cdot)}$ and $k'_{\mathrm{L}(\cdot)}(\mathbf{y}, \mathbf{d}) = 1 - f_{\mathrm{L}(\cdot)(\mathbf{y},\mathbf{d})} = k_{\mathrm{L}(\cdot)} V_{\mathrm{L}(\cdot)}$, where $\mathbb{I}[\cdot]$ is the indicator function. Similar to f, k' can be an also be expressed as as a function of $\boldsymbol{\epsilon}$; further, $k = k'/V$. Now, we will show that the kernels are indeed valid kernels, which, for the purposes of GABC, need only satisfy $\int k(\mathbf{y}, \mathbf{d})\, \mathrm{d}\mathbf{y} = 1$ (Fearnhead and Prangle 2012). First, note that the kernels are all bounded and non-negative over their respective supports. For $k'_{\mathrm{E}(\cdot)}$, non-negativity and boundedness follows from the the fact that p-values are non-negative and bounded by 1; i.e., $p_i \in [0, 1]\ \forall i \in \{1, 2, \ldots, N_m\}$. For $k'_{\mathrm{L}(\cdot)}$, non-negativity and boundedness stems from the pdfs $\pi_{E_i}(e_i)$. Moreover, $k'_{\mathrm{E}(\cdot)}$ has compact support around $\mathbf{d}$. Therefore, $k'_{\mathrm{E}(\cdot)}$ is measurable, since all closed subsets of $\mathbb{R}^{N_m}$ are measureable. Similarly, $k'_{\mathrm{L}(\cdot)}$ must be integrable since the $\pi_{E_i}(e_i)$ are integrable. Thus, $k'_{(\cdot)}$ is integrable (Durrett 2019) and it follows that $V_{(\cdot)} < \infty$. Since $k_{(\cdot)}$ is nothing but a re-scaled version of $k'_{(\cdot)}$ with unit hyper-volume, $k_{(\cdot)}$ is a valid density kernel.

MODEL FALSIFIED ABC THROUGH A BAYESIAN REINTERPRETATION OF MODEL FALSIFICATION

Fig. 5 shows the process of model falsification when the models are sampled according to a prior; this process resembles the workflow of standard rejection sampling based ABC where the falsifier plays the role of the discrepancy metric. Thus, the set of unfalsified models

$$\boldsymbol{\Theta}_u = \left\{\boldsymbol{\theta} \mid f_{(\cdot)}(\mathbf{y}, \mathbf{d}) \leq \kappa_{(\cdot),\phi} \text{ where } \mathbf{y} \sim \pi(\boldsymbol{y}|\boldsymbol{\theta})\right\}, \tag{15}$$

yields an approximation to the posterior pdf. The approximation will depend on the falsifier used, the target identification probability and the marginal densities assumed to model the residual errors. Let,

$$\mathcal{A}_{\phi,\mathbf{d}}(\boldsymbol{y}) = \left\{\boldsymbol{y} \in \mathfrak{D} | f_{(\cdot)}(\boldsymbol{y}, \mathbf{d}) \leq \kappa_{(\cdot),\phi}\right\}, \tag{16}$$

be the set/region of predictions that are unfalsified by $f_{(\cdot)}$ for a specified target identification probability ϕ. Eq. (16) leads to an approximate posterior pdf, denoted herein as $\pi_{\text{ABC}}(\boldsymbol{\theta}|\mathbf{d})$, that can be found using Eq. (4) as follows

$$\pi_{\text{ABC}}(\boldsymbol{\theta}|\mathbf{d}) \propto P(\boldsymbol{y} \in \mathcal{A}_{\phi,\mathbf{d}})\pi(\boldsymbol{\theta}). \tag{17}$$

Eq. (17) provides a Bayesian interpretation to model falsification. More precisely, model falsification is nothing but ABC performed with model falsifiers as discrepancy metrics and the set of unfalsified models may be considered as realizations from an approximate posterior pdf. Herein, we will refer to the schematic of Fig. 5 as *model falsified ABC*. In a similar vein, model falsified GABC is performed using the kernels based on model falsifiers and is called herein *model falsified GABC*.

Can the true posterior be recovered?

Consider falsifiers — like f_{ES}, f_{LS} and f_{LB} but not f_{EB} — that satisfy the property $f(\mathbf{y}, \mathbf{d}) = 0$ if and only if $\mathbf{y} = \mathbf{d}$. In such a case, the true posterior can theoretically be recovered by setting the target identification probability to zero. In that case, $\mathcal{A}_{\phi,\mathbf{d}} \equiv \mathcal{A}_{\mathbf{d}}$ when $\phi = 0$. Thus, model falsification using the falsifiers f_{ES}, f_{LS} and f_{LB} corresponds to Bayesian inference when $\phi = 0$. However, the true posterior cannot be recovered practically because acceptance ratios drop as $\phi \rightarrow 0$.

A special case for the likelihood domain falsifier

Consider a case where the measurements are corrupted with independent and identically distributed (IID) additive noise $\boldsymbol{\eta}$; i.e., $\mathbf{d} = \mathbf{y} + \boldsymbol{\eta}$. This measurement model is common in many applications. In this case, since the probability distribution of the η_i are the same as those of the ϵ_i, $k_{\mathrm{L}} = \pi(\mathbf{d}|\boldsymbol{y})$ and, as a result, $\ell_{\mathrm{ABC}}(\mathbf{d}|\boldsymbol{\theta}) = \ell(\mathbf{d}|\boldsymbol{\theta})$. However, $\ell(\mathbf{d}|\boldsymbol{\theta})$ may still be intractable or difficult to compute, which is the primary reason for adopting ABC and not using Bayesian inference. Moreover, without k_{L} being compactly supported, GABC using k_{L} is equivalent to performing Bayesian inference. Thus, we do not assign a compact support to k_{L} to retain the aforementioned property.

APPLICATION OF MODEL FALSIFIED (G)ABC TO PARAMETER INFERENCE

In this section, model falsified (G)ABC is applied to two inverse problems of parameter estimation — an illustrative toy example for which the likelihood cannot be calculated in closed form, and a system identification example wherein the parameters of a cubic-quintic dynamical system are estimated from noisy measurements. Some pointers and resources that may be helpful for implementing model falsified (G)ABC approaches are given in Appendix II.

A toy example

To show how model falsified ABC can be used to approximate the posterior pdf, we adopt the following simple example. Consider the model

$$d_i = y_i + \eta_i, \quad y_i = (0.9 + 0.2\beta_i)\,\theta, \qquad i = 1, 2 \tag{18}$$

where β_1 and β_2 are IID Beta(2,2) random variables, and η_1 and η_2 are IID zero-mean Gaussian random variables with standard deviation $\sigma_\eta = 0.05$. For this example, θ is assigned a standard normal prior with a true value of 1 that is denoted as θ_{true} herein. Also, $\boldsymbol{y} = [y_1, y_2]^{\mathrm{T}}$ with $y_i|\theta$ being Beta distributed, and $\mathbf{d} = [d_1, d_2]^{\mathrm{T}}$ with $d_i|y_i$ being Gaussian distributed. The goal is to estimate the parameter θ from the two noisy observations $\mathbf{d} = [0.921, 1.017]^{\mathrm{T}}$. The likelihood function $\ell(\mathbf{d}|\theta)$ is given by

$$\ell(\mathbf{d}|\theta) = \int \pi(\mathbf{d}|\mathbf{y})\pi(\mathbf{y}|\theta)\,\mathrm{d}\mathbf{y} = \iint \pi(d_1|y_1)\pi(d_2|y_2)\pi(y_1|\theta)\pi(y_2|\theta)\,\mathrm{d}y_1\mathrm{d}y_2. \tag{19}$$

The likelihood function and the posterior pdf cannot be computed analytically, which makes the application of Bayesian inference challenging. However, given the simple nature of the problem, Bayesian inference can still be performed by computing $\ell(\mathbf{d}|\boldsymbol{\theta})$ from Eq. (19) using Monte Carlo simulation (Kroese et al. 2013), and the parameter θ can be estimated using Markov-chain Monte Carlo (MCMC) (Kroese et al. 2013). The posterior mean and coefficient of variation (COV) of θ were found to be 0.9711 and 0.0023 respectively. The statistics were estimated using 1000 realizations from a single MCMC chain where realizations were accepted after an initial burn period of 5000 and a lag of 20. Herein, we choose the error residuals as IID zero-mean Gaussian random variables and vary the standard deviation σ_ϵ. (In Section SM2 in the Supplemental Material and in (Dasgupta 2023), we study the effect of misspecifying the $\pi_{E_i}(e_i)$ by assuming the error residuals to be Laplace distributed.)

Estimating θ using model falsified ABC

First, we estimate θ using model falsified ABC where the falsifiers act as discrepancy metrics. We begin by assuming that σ_η is known and set $\sigma_\epsilon = \sigma_\eta$. The target identification probability is varied between $\phi = 0.99$ and 0.30. Fig. 6 shows the approximate posterior pdf obtained using different falsifiers at three representative values of ϕ (these pdfs were estimated from the unfalsified realizations of θ using the kernel density estimation technique of MATLAB (The Mathworks, Inc. 2021)). Fig. 7 shows the posterior mean and coefficient of variation (COV) of the approximate posterior pdfs. The estimate for the posterior mean improves as ϕ is reduced since the threshold $\kappa_{(\cdot),\phi}$ decreases (Barber et al. 2015). Moreover, as ϕ is decreased, more models are falsified, which results in a decrease in the approximate pdf's COV. The behavior of the various falsifiers is also evident in Fig. 7. Recall that f_{EB} falsifies more models as compared to f_{ES} for the same value of ϕ. Similarly, the likelihood domain falsifiers unfalsify more models as compared to the error domain falsifiers for the same value of ϕ. Hence, the COV of the approximate pdf is less for f_{EB} as compared to f_{ES}, and the COV of the likelihood domain falsifiers is more than those of the error domain falsifiers.

The assumed distributions of the residual error also play an important role in the approximation of the posterior pdf, and may possibly be unknown or poorly estimated. Different choices of σ_ϵ lead to different approximations of the posterior pdf. Choosing $\sigma_\epsilon > \sigma_\eta$ means the noise in the measurements is overestimated, causing more models to be unfalsified for the same value of ϕ, while $\sigma_\epsilon < \sigma_\eta$ leads to the falsification of more models. Thus, assuming $\sigma_\epsilon > \sigma_\eta$ is equivalent to setting a looser tolerance κ and vice versa. Fig. 8 shows the approximate posterior pdf obtained using three different values of σ_ϵ that correspond to assuming double, equal and half signal to noise ratios, for the falsifier f_{ES} when $\phi = 0.90$. The mean and COV of the approximate posterior pdfs for $\boldsymbol{\theta}$ are also shown in Fig. 8. For the same value of ϕ, the COV of the posterior samples reduces with σ_ϵ due to more models being falsified. Note that the same level of approximation is possible from the three different assumptions about the residual errors albeit at three different levels of ϕ. Thus, a good approximation to the posterior pdf can be obtained even in the case where the statistics of the assumed residual errors are poorly designed.

Estimating θ using model falsified GABC

Now, θ is estimated using the GABC approach with kernels based on falsifiers. The target identification probability ϕ was fixed to 0.99 to maintain healthy acceptance ratios. As before, we assume the error residuals to be IID zero-mean Gaussian random variables with standard deviation $\sigma_\epsilon = \sigma_\eta$. The approximate posterior pdfs obtained using the three kernels, shown in the left plot in Fig. 9, exhibit a good match with the true posterior pdf from Bayesian inference. For the kernels k_{ES}, k_{EB} and k_{L}, the mean of the approximate posterior of θ was found to be 0.9686, 0.9694 and 0.9686, while the approximate posterior had a COV of 0.0029, 0.0030 and 0.0021, respectively. Among the three kernels, k_{L} provides the best approximation to the true posterior pdf. This is expected since the kernel k_{L} accurately captures $\pi(\mathbf{d}|\boldsymbol{y})$. In fact, ABC using the kernel k_{L} should ideally have resulted in the same distribution, and the small deviation from the true posterior statistics may be attributed to Monte Carlo error. The assumed standard deviation σ_ϵ for the residual errors plays a more crucial role when falsifiers are used as kernels as it controls the effective bandwidth of the kernels. The approximate posterior pdfs obtained using model falsified GABC with the kernel k_{ES} with different values of σ_ϵ are shown in Fig. 9. A lower value of σ_ϵ causes the uncertainty to be underestimated. Thus, when using falsifiers as kernels, the residual errors should be carefully designed such that the resulting approximation is useful.

Application: system identification of a cubic-quintic oscillator

In this example, model falsified (G)ABC is used to infer the system parameters of a cubic-quintic dynamical system. Duffing oscillators with cubic and quintic nonlinear terms can be used to model dynamical systems that arise in many real world applications (Elías-Zúñiga 2013). The cubic-quintic system has also been studied in the context of parameter inference using ABC approaches in previous works (Abdessalem et al. 2018; Abdessalem et al. 2019). The equation of motion of the time invariant cubic-quintic system is given by

$$m\ddot{x}(t) + c\dot{x}(t) + kx(t) + k_3x^3(t) + k_5x^5(t) = w(t). \tag{20}$$

where m, c and k are the mass, damping and linear stiffness coefficients, while k_3 and k_5 are the non-linear cubic and quintic stiffness coefficients, respectively. $x(t)$, $\dot{x}(t)$ and $\ddot{x}(t)$ are the displacement, velocity and acceleration response of the system, respectively, at time instant t. For this example, all quantities are considered non-dimensional. The true values of the parameters are: $m = 1$, $c = 0.05$, $k = 50$, $k_3 = 10^3$ and $k_5 = 10^5$. The system is assumed to start from rest and is excited by a white noise excitation $w(t)$ with mean zero and instantaneous variance 10 units. The excitation used to generate the synthetic response of the system is shown in Fig. 10a; the resulting time history of the system displacement is shown in Fig. 10b. The system response is generated by integrating Eq. (20) up to $t = 5$ using the *solve_ivp* function from the `SciPy` package (Virtanen et al. 2020) with a time step of $\Delta t = 0.01$. Measurements $\mathbf{d}$ are recorded at a sampling frequency of 25 Hz; ignoring the first measurement at $t = 0$, $N_m = 125$. The measurements are corrupted by an additive zero-mean Gaussian noise with standard deviation equal to 1% of the root-mean-square (RMS) of the true displacement response. The measurements are also shown in Fig. 10(b).

The unknown parameters' priors, chosen following (Abdessalem et al. 2018), are: $m \sim \mathcal{U}(0.1, 10)$, $c \sim \mathcal{U}(0.0005, 0.5)$, $k \sim \mathcal{U}(5, 500)$, $k_3 \sim \mathcal{U}(10^2, 10^4)$ and $k_5 \sim \mathcal{U}(10^4, 10^6)$, where $X \sim \mathcal{U}(a, b)$ means that the random variable X is uniformly distributed between a and b. Throughout this example, we assume the residual errors are IID zero-mean Gaussian random variables with standard deviation equal to 5% of the RMS of the measured response. We found implementing model falsified (G)ABC to be computationally inefficient because the priors are relatively diffuse, making very small the fraction of unfalsiable models. So we use a sequential Monte Carlo (SMC) algorithm, proposed by Toni et al. (2009), to sample from the ABC posterior. The SMC technique for ABC is briefly described in section III. Moreover, we implement SMC using the open-source Python toolbox `pyABC` (Klinger et al. 2018). Among other things, `pyABC` allows parallel implementation of SMC, as well as adaptively chosen intermediate thresholds in the SMC process.

We note that the model adopted in this example is deterministic; i.e., given a realization of the parameter vector $\boldsymbol{\theta} = [m, c, k, k_3, k_5]^{\mathrm{T}}$, the prediction from it is always the same. We consider this example because the likelihood function is tractable when the properties of the measurement noise process are known and, as a result, Bayesian inference can be adopted to infer the parameter vector $\boldsymbol{\theta}$. In fact, model falsified GABC performed with the kernel k_{L} is equivalent to Bayesian inference in such cases. Thus, this example offers an opportunity to compare the performance of model falsified (G)ABC with Bayesian inference.

Parameter inference using model falsified ABC

First, the unknown parameters of the cubic-quintic system are estimated using model falsified ABC with the target identification probability ϕ set to 0.99. The SMC scheme is run with 1000 particles at every population (Fig. SM4 in the Supplementary Material shows the evolution of the posterior mean of the different system parameters through the populations of SMC for different falsifiers (Dasgupta 2023)). Table 2 shows the average relative error between the posterior mean and the true value for each parameter and the COV associated with the parameter estimates obtained using the different falsifiers averaged across 10 independent runs (detailed summary statistics of the approximate posterior distributions are reported in Table SM1 in the Supplemental Material). The results show that model falsified ABC using the error domain falsifiers performs very well, with relative errors of the estimated m, k and k_5 below 10%. The corresponding likelihood domain falsifiers perform slightly poorer for the same value of ϕ. However, all four falsifiers have difficulty in identifying c and k_3. Plots of the approximate pdfs of the various system parameters corresponding to the different falsifiers can be seen in Fig. 11. The approximate pdfs were found to peak around the true values of the parameters for the error domain falsifiers: a qualitative indication that the inference is good.

Fig. 11 shows the approximate pdfs of the various system parameters corresponding to the different falsifiers. The pdfs in Fig. 11 were estimated from the unfalsified models in the last population of the SMC algorithm using kernel density estimation. The posterior mean of the parameters is collectively denoted the *identified model* herein. The approximate pdfs also peak around the true values of the parameters for the error domain falsifiers: a qualitative indication that the inference is good.

Fig. 12(a) shows the predicted response when the identified model from each falsifier is excited using the random Gaussian excitation shown in Fig. 10(a); Column 2 in Table 3 shows the corresponding normalized root-mean-square-error (RMSE), which is denoted ϵ_{RMSE} herein. The predictive capability of the identified systems are further tested by evaluating the response to a different test excitation and comparing it to the true response. A harmonic excitation $\tilde{w}(t) = 10 \cdot \sin(\omega_{\mathrm{f}} t)$ with $\omega_{\mathrm{f}} = 10$ is used as the test excitation. Fig. 12(b) shows the predicted response of the identified models under the test excitation while their respective ϵ_{RMSE} values are tabulated in Column 3 of Table 3. The better estimation capability of the error domain falsifiers also translates to better predictive capabilities of the identified models; ϵ_{RMSE} is lower across both excitations for the error domain falsifiers. However, the comparatively better performance of the error domain falsifiers comes at an increased computational cost. The average number of model evaluations necessary to sample from the approximate posterior corresponding to each falsifier is shown in Column 4 of Table 3: model falsified ABC using the error domain falsifiers requires an order of magnitude more model simulations than the likelihood domain falsifiers to reach the same threshold. The best performing falsifier is f_{EB}, with lower relative errors in the posterior mean of all system parameters except k_5 and lower ϵ_{RMSE} from the identified model under both excitations, although it is slightly less computationally efficient as compared to the other falsifiers.

Parameter inference using model falsified GABC

Now, we use model falsified GABC to estimate $\boldsymbol{\theta}$. Kernels k_{ES} and k_{EB} are assigned compact supports by setting $\phi = 0.99$. A modified SMC algorithm (see III) was used to perform model falsified GABC. As before, we set $N = 1000$ as the population size. Unfortunately, a limit of 10^8 model runs precluded GABC with k_{L} from converging with this setting. (It was only possible to sample from $k_{\mathrm{L}}^{1/12.5}$. For reference, sampling from k_{L}^{0} and k_{L} is equivalent to sampling from the prior $\pi(\boldsymbol{\theta})$ and Bayes' posterior $\pi(\boldsymbol{\theta}|\mathbf{d})$, respectively.) Thus, we are only able to report the results corresponding to an annealed posterior pdf (specifically, $k_{\mathrm{L}}^{1/12.5}$).

The relative error of the posterior mean of the system parameters obtained using model falsified GABC with various kernels is provided in Table 4. The COV values of the posterior estimates is also provided in Table 4 (more detailed summaries of the approximate posterior distributions obtained using GABC with various kernels is provided in Table SM2 in the Supplemental Material and in (Dasgupta 2023)). The performance of the model falsified GABC approach is similar to model falsified ABC. As before, the true parameter values lie within the inter-quartile ranges, and, as shown in Fig. 13, the approximate posterior pdfs peak around the true values. This shows that inference using model falsified GABC is of good quality. Similarly, predictions to both $w(t)$ and $\tilde{w}(t)$ from the identified models are shown in Fig. 14. The predictions agree well with the true response, as evidence by the low normalized RMSE values in Table 5, which means that the identified models can generalize well. The kernel k_{ES} performs better than k_{EB} at estimating all parameters except for m and c. k_{ES} also outperforms k_{EB} when the prediction capabilities of the identified models are compared. However, as evident from Column 4 of Table 5, model falsified GABC with k_{ES} is more computationally expensive. However, model falsified GABC with k_{L}, i.e., Bayesian inference, is computationally prohibitive in this case. The results provide empirical evidence that model falsified (G)ABC can be a computationally efficient alternative to Bayesian inference when the prior density is diffused. These findings are consistent with those reported by Abdessalem et al. (2018).

MODEL CLASS SELECTION WITH THE MODEL FALSIFIED (G)ABC FRAMEWORKS

In many physical applications, the underlying model that describes the relationship between the uncertain parameters and the observations, or some part thereof, is unknown or must be chosen from a set of probable model classes (defined as a collection of parameterized models). Consider the set $\mathscr{M} = \{\mathcal{M}_1, \mathcal{M}_2, ..., \mathcal{M}_K\}$ of model classes that all describe the same phenomena. The objective of model class selection is to determine which model class(es) can predict the observations $\mathbf{d}$. Bayesian model class selection refers to the method of selecting model classes based on the posterior model class probabilities, which are denoted herein as $P(\mathcal{M}_k|\mathbf{d})\ \forall k = 1, 2, \ldots, K$. Also, let $\boldsymbol{\theta}_k \in \boldsymbol{\Theta}_k$ be the parameter vector associated with the model class $\mathcal{M}_k$. Then Bayes' theorem gives us

$$P(\mathcal{M}_k|\mathbf{d}) \propto \pi(\mathbf{d}|\mathcal{M}_k)P(\mathcal{M}_k) \tag{21}$$

where

$$\pi(\mathbf{d}|\mathcal{M}_k) = \int_{\boldsymbol{\Theta}_k} \underbrace{\int_{\mathfrak{D}} \pi(\mathbf{d}|\boldsymbol{y}_k, \boldsymbol{\theta}_k, \mathcal{M}_k)\pi(\boldsymbol{y}_k|\boldsymbol{\theta}_k, \mathcal{M}_k)\pi(\boldsymbol{\theta}_k|\mathcal{M}_k)\ \mathrm{d}\boldsymbol{y}}_{\ell(\mathbf{d}|\boldsymbol{\theta}_k, \mathcal{M})}\ \mathrm{d}\boldsymbol{\theta} \tag{22}$$

is commonly known as the model evidence or marginal likelihood and $P(\mathcal{M}_k)$ is the prior probability assigned to the model class $\mathcal{M}_k$. Model falsified ABC can be used to perform model class selection simply by setting $\pi(\mathbf{d}|\boldsymbol{y}_k, \boldsymbol{\theta}_k, \mathcal{M}_k) = \mathcal{I}_{\mathcal{A}_{\phi,\mathbf{d}}}(\boldsymbol{y}_k; \boldsymbol{\theta}_k, \mathcal{M}_k)$ in Eq. (22), which leads to the approximate posterior model class probabilities

$$P_{\mathrm{ABC}}(\mathcal{M}_k|\mathbf{d}) \propto \left[\int_{\boldsymbol{\Theta}_k} P(\boldsymbol{y}_k \in \mathcal{A}_{\phi,\mathbf{d}})\pi(\boldsymbol{\theta}_k|\mathcal{M}_k)\ \mathrm{d}\boldsymbol{\theta}_k\right] P(\mathcal{M}_k). \tag{23}$$

Similar modifications can also be made for model falsified GABC. Also note that, for the special cases discussed in Section 4, the posterior model class probabilities can be recovered by setting $\phi = 0$.

Model class selection for base isolation devices using model falsified (G)ABC

Consider the base isolated shear frame structure shown in Fig. 15a. In this example, which is adopted from (De et al. 2018), the appropriate model for the isolation layer is to be determined. Identifying the behavior of isolation-layer devices is important for predicting system responses that may, in turn, inform design choices and control strategies. The equations of motion of the system are

$$\boldsymbol{M}_\mathrm{s}\ddot{\boldsymbol{X}}_\mathrm{s} + \boldsymbol{C}_\mathrm{s}\dot{\boldsymbol{X}}_\mathrm{s} + \boldsymbol{K}_\mathrm{s}\boldsymbol{X}_\mathrm{s} = -\boldsymbol{M}_\mathrm{s}\mathbf{1}\ddot{x}_g + \boldsymbol{C}_\mathrm{s}\mathbf{1}\dot{x}_\mathrm{b} + \boldsymbol{K}_\mathrm{s}\mathbf{1}x_\mathrm{b} \tag{24}$$

$$m_\mathrm{b}\ddot{x}_\mathrm{b} + \mathbf{1}^\mathrm{T}\boldsymbol{C}_\mathrm{s}\mathbf{1}\dot{x}_\mathrm{b} + \mathbf{1}^\mathrm{T}\boldsymbol{K}_\mathrm{s}\mathbf{1}x_\mathrm{b} + f_\mathrm{b} = -m_\mathrm{b}\ddot{x}_\mathrm{g} + \mathbf{1}^\mathrm{T}\boldsymbol{C}_\mathrm{s}\dot{\boldsymbol{X}}_\mathrm{s} + \mathbf{1}^\mathrm{T}\boldsymbol{K}_\mathrm{s}\boldsymbol{X}_\mathrm{s} \tag{25}$$

where

$$\boldsymbol{M}_\mathrm{s} = \begin{bmatrix} m_1 & 0 & 0 \\ 0 & m_2 & 0 \\ 0 & 0 & m_3 \end{bmatrix} \quad \text{and} \quad \boldsymbol{K}_\mathrm{s} = \begin{bmatrix} k_1 + k_2 & -k_2 & 0 \\ -k_2 & k_1 + k_2 & -k_3 \\ 0 & -k_3 & k_1 + k_2 \end{bmatrix} \tag{26}$$

are the mass and stiffness matrices of the superstructure, respectively; m_b and c_b are the base mass and isolation layer linear damping coefficient, respectively; $\boldsymbol{X}_\mathrm{s} = [x_1, x_2, x_3]^\mathrm{T}$ are the floor displacements relative to the ground; x_b is the base displacement relative to the ground; and $\mathbf{1}$ is a column vector of all ones. A proportional Rayleigh damping is assumed for the superstructure; i.e., $\boldsymbol{C}_\mathrm{s} = \beta_1\boldsymbol{M}_\mathrm{s} + \beta_2\boldsymbol{K}_\mathrm{s}$ with 3% damping in the first two modes. We also choose $m_1 = m_2 = m_3 = 300$ Mg and $k_1 = k_2 = k_3 = 40$ MN/m, respectively. The base mass $m_\mathrm{b} = 500$ Mg. f_b, representing the effect of the isolation layer damping and restoring force, depends on the isolation layer model adopted. The total mass of the structure is $m = m_\mathrm{b} + m_1 + m_2 + m_3 = 1400$ Mg.

Model classes for the base isolation device

(1) Nonlinear model classes: In this study, we consider two nonlinear model classes that can approximate the behavior of the isolation layer — a bilinear hysteresis model and a Bouc-Wen

hysteresis model (Wen 1976) denoted herein as $\mathcal{M}_1$ and $\mathcal{M}_2$, respectively. Representative force displacement behaviors for both model classes can be seen in Fig. 15b. For both model classes, $\mathrm{k}_{\mathrm{pre}}$, k_{post} and Q_{y} are used to denote pre-yield and post-yield stiffnesses, and the yield force, respectively. Now, the force f_{b} exerted by the isolation layer can be expressed as

$$f_{\mathrm{b}} = c_{\mathrm{b}}\dot{x}_{\mathrm{b}} + k_{\mathrm{post}}x_{\mathrm{b}} + q_{\mathrm{y}}z \tag{27}$$

where $q_{\mathrm{y}}z$ represents the nonelastic force and z is an evolutionary variable. In nonlinear model classes, $q_{\mathrm{y}} = Q_{\mathrm{y}}(1-r_{\mathrm{k}})$ where $r_{\mathrm{k}} = k_{\mathrm{post}}/k_{\mathrm{pre}}$ is the hardness ratio and z is an evolutionary variable whose evolution is governed by

$$\dot{z} = A\dot{x}_{\mathrm{b}} - \beta\dot{x}_{\mathrm{b}}|z|^{n_{\mathrm{pow}}} - \gamma z|\dot{x}_{\mathrm{b}}||z|^{n_{\mathrm{pow}}-1} \tag{28}$$

where $A = 2\beta = 2\gamma = k_{\mathrm{pre}}/Q_{\mathrm{y}}$ is chosen to ensure that z is contained within $[-1, 1]$ and the loading and unloading stiffnesses remain equal (Ramallo et al. 2002). We adopt $n_{\mathrm{pow}} = 1$ for the Bouc-Wen model class, and $n_{\mathrm{pow}} = 100$ for the bilinear model class (De et al. 2018).

(2) Linear model classes: A few linear model classes are considered as alternates to the nonlinear model classes described above. The force displacement behavior of one linear model class is also shown in Fig. 15b. Linear model classes are considered because they can be computationally efficient alternatives that are simpler for engineering design. In linear model classes, the force exerted by the isolation layer is represented as

$$f_{\mathrm{b}} = [c_{\mathrm{b}} + c_{\mathrm{eq}}]\dot{x}_{\mathrm{b}} + k_{\mathrm{eq}}x_{\mathrm{b}} = \left[c_{\mathrm{b}} + 2\zeta_{\mathrm{eq}}\sqrt{k_{\mathrm{eq}}m_{\mathrm{b}}}\right]\dot{x}_{\mathrm{b}} + k_{\mathrm{eq}}x_{\mathrm{b}}. \tag{29}$$

The American Association of State Highway and Transportation Officials (AASHTO) and the Japanese Public Works Research Institute (JPWRI) recommend

$$k_{\mathrm{eq}} = \frac{k_{\mathrm{pre}}}{\rho}\left[1 + r_{\mathrm{k}}(\rho - 1)\right] \quad \text{and} \quad \zeta_{\mathrm{eq}} = \frac{2(1 - r_{\mathrm{k}})(1 - \rho^{-1})}{\pi\left[1 + r_{\mathrm{k}}(\rho - 1)\right]}, \tag{30}$$

with $\rho = r_\mathrm{d}$ and $0.7r_\mathrm{d}$ for the AASHTO and JPWRI model classes, respectively (Hwang and Chiou 1996), where $r_\mathrm{d} = x_\mathrm{d}k_\mathrm{pre}/Q_\mathrm{y}$ is the shear ductility ratio. A modified AASHTO model class is also considered, for which $\rho = r_\mathrm{d}$ and multiplicative correction factors of $r_\mathrm{d}^{0.58}/(6 - 10r_\mathrm{k})$ and $\left[1 - 0.737(r_\mathrm{d} - 1)/r_\mathrm{d}^2\right]^{-2}$ are applied to ζ_eq and k_eq, respectively (Hwang and Chiou 1996). Further, based on recommendations from the California Department of Transportations (Caltrans) (Hwang and Chiou 1996), we also consider

$$\zeta_\mathrm{eq} = 0.0587(r_\mathrm{d} - 1)^{0.371} \quad \text{and} \quad k_\mathrm{eq} = k_\mathrm{pre}\left[1 + \ln\left\{1 + 0.13(r_\mathrm{d} - 1)^{1.137}\right\}\right]^{-2}. \tag{31}$$

The AASHTO, JPWRI, modified AASHTO and Caltrans model classes are herein denoted as $\mathcal{M}_3$, $\mathcal{M}_4$, $\mathcal{M}_5$ and $\mathcal{M}_6$, respectively. Thus, in total, there are $K = 6$ model classes, to which uniform prior probabilities are assigned; i.e., $P(\mathcal{M}_k) = K^{-1}\ \forall \mathcal{M}_k \in \mathscr{M}$. Additionally, the parameters k_post, c_b, r_k, r_d and Q_y are assumed to be uncertain across the different model class. The parameter priors are tabulated in Table 6. Note that the parameter r_d is not necessary for the nonlinear model classes while the linear model classes do not require the parameter Q_y.

Synthetic measurements and error residual density

In this example, we choose the N–S El Centro, California, earthquake record during the May 18, 1940, Imperial Valley earthquake sampled at 50 Hz, that had a peak acceleration of 3.42 m/s^2, as the base excitation $\ddot{x}_\mathrm{g}$. A model from the Bouc-Wen model class is used to generate the synthetic data set. The parameters of the truth model are tabulated in Table 6; the hysteresis curve of the evolutionary variable z with respect to base displacement x_b, along with the absolute acceleration at the base isolation layer of the truth model, are shown in Fig. 16. The absolute acceleration $\ddot{x}_\mathrm{b}^\mathrm{a}$ of the base layer is sampled at 20 Hz for 30 s ($N_m = 600$), to which we add Gaussian noise with standard deviation equal to 10% of the RMS of the actual response to generate noisy measurements. The error residual densities are also assumed to be Gaussian with a slightly higher standard deviation set equal to 15% of the RMS of the measurements $\mathbf{d}$.

Model class selection using model falsified ABC

In this example, we again use the SMC algorithm to perform model class selection; the posterior model class probability is proportional to the relative frequency of different model classes in the last population of the SMC algorithm (Toni et al. 2009; Abdessalem et al. 2018). We set the population size for the SMC algorithm to $N = 5000$. Fig. 17 shows the posterior model class probabilities of each model class. All falsifiers are able to correctly select the Bouc-Wen model class ($\mathcal{M}_2$). The error-domain falsifiers reject all other model classes for all values of ϕ that we consider. In comparison, the likelihood domain falsifiers are more conservative in falsifying models and, as a result, some posterior mass is assigned to the linear model classes when $\phi = 0.99$. As ϕ is decreased to 0.95, the posterior probability of the linear model classes drop to zero. Subsequently, as we decrease ϕ to 0.90, the bilinear model class $\mathcal{M}_1$ is no longer assigned any posterior mass.

The relative error between the posterior mean of the parameters of the Bouc-Wen model class $\mathcal{M}_2$ obtained using different falsifiers and the true value is provided in Table 7 (a more detailed summary of the approximate posterior distributions can be found in Table SM3, and the corresponding approximate pdfs are shown in Fig. SM5, in the Supplemental Material and in (Dasgupta 2023)). In this case also, the error domain falsifiers, owing to fact that they are more restrictive at the same level of ϕ, are better at estimating the parameters, with the performance of f_{EB} being marginally better than f_{ES}. The parameters are well estimated with the range between the 5$^{\text{th}}$ and 95$^{\text{th}}$ percentiles containing the true value for all parameters except k_{post}. All falsifiers find it difficult to estimate parameter c_{b}.

Fig. 18a shows the approximate posterior predicted mean absolute base acceleration under the El Centro excitation for different falsifiers. Columns 2 and 4 in Table 8 show the normalized RMSE between the true and posterior mean absolute base acceleration response, and normalized error between the true and posterior maximum absolute base acceleration response, respectively, under the El Centro excitation. Table 8 shows that model falsified ABC is able to make good predictions of the maximum response. The response of the structure after the ground motion subsides is not predicted as well as the initial response because the damping properties of the isolation layer are not well estimated. The performance of the estimated parameters under a new excitation is also studied. For this, the base isolated structure is subjected to the July 2019 Ridgecrest, California earthquake. The ground motion recorded by Channel 1 (90° component) at Tower 2 is used as the ground excitation, the peak acceleration for which was reported to be 3.90 m/s^2 (Center for Engineering Strong Motion Data 2019; Strong Motion Virtual Data Center 2019). Fig. 18b shows the approximate posterior predicted mean absolute base acceleration of the structure under the Ridgecrest ground excitation for different falsifiers. The normalized errors in the predicted response, shown in Columns 3 and 5 of Table 8, indicate that the estimated parameters also generalize well to different excitations. In this example as well, the relative order between the model falsifiers in terms of the number of model simulations was similar.

Model class selection using model falsified GABC

Model class selection using the falsifier based kernels are investigated in the context of this example. Again, the SMC algorithm with a population size $N = 5000$ is used to perform model falsified GABC. We fix $\phi = 0.99$ for the kernels k_{ES} and k_{EB}. Fig. 19 shows the approximate posterior probabilities of the different model class evolving with the populations of the SMC algorithm. Model falsified GABC with all the kernels estimate $P(\mathcal{M}_2|\mathbf{d}) = 1$ at the final population, thereby choosing the correct model class.

The relative errors between the posterior means and the true parameter values are reported in Table 9. (The summary statistics of the approximate posterior distribution of the parameters of the Bouc-Wen model class are tabulated in Table SM4 and the corresponding approximate posterior pdfs, estimated using kernel density estimation, are shown in Fig. SM6 in the Supplemental Material and in (Dasgupta 2023).) In this example, the approximate posterior pdfs, obtained using model falsified ABC and GABC, do not peak around the true parameter values due to the presence of large noise in the measurements. Bayesian inference can overcome this challenge because the likelihood model is correctly specified by k_{L}. The kernel k_{ES} performs marginally better than k_{B}, both in terms of the predicted uncertainty and relative errors of the estimated parameters. Unlike the previous example, the SMC algorithm converged for the kernel k_{L}, and model falsified GABC with k_L, or Bayesian inference, provides the best results. (The approximate posterior predicted mean absolute base acceleration obtained using model falsified GABC with different kernels under the El Centro and Ridgecrest earthquake excitations are omitted here, as they are similar to Fig. 18, but are included in Figs. SM7a and SM7b in the Supplemental Material and in (Dasgupta 2023).) The normalized RMSE between the true and predicted responses is tabulated in Table 10. Bayesian inference outperforms model falsified GABC with the falsification kernels as well, when compared in terms of predictive quality of the identified model. However, the number of populations required for the model falsified GABC with k_L to converge is significantly higher than the other kernels, which means that Bayesian inference is a more computationally expensive alternative to model falsified GABC.

MODEL FALSIFIER BASED KERNEL REGRESSION FOR PARAMETER ESTIMATION AND RESPONSE PREDICTION

In this section, we introduce kernel regression using model falsifier based kernels: a non-parametric approach to parameter estimation and response prediction. Let, $g(\boldsymbol{\theta})$ be a function of the underlying uncertain parameter $\boldsymbol{\theta}$. The Nadaraya-Watson estimator for the conditional expectation of $g(\boldsymbol{\theta})$ given the observations $\mathbf{d}$, which we denote as $\hat{g}_{\mathrm{NW}}$, obtained using a kernel $k_{(\cdot)}$ is given as

$$\hat{g}_{\mathrm{NW}} = \frac{\sum_{i=1}^{N} g(\boldsymbol{\theta}^{(i)}) k_{(\cdot)}(\mathbf{y}^{(i)}, \mathbf{d})}{\sum_{i=1}^{N} k_{(\cdot)}(\mathbf{y}^{(i)}, \mathbf{d})}, \tag{32}$$

where $\mathbf{y}^{(i)}$ is a prediction from $\boldsymbol{\theta}^{(i)}$ (a realization drawn from $\pi(\boldsymbol{y}|\boldsymbol{\theta}^{(i)})$) corresponding to $\mathbf{d}$ (Blum 2010). The Nadaraya-Watson estimator can be used to estimate the posterior mean of $\boldsymbol{\theta}$ by setting $g(\boldsymbol{\theta}) = \boldsymbol{\theta}$ to obtain

$$\hat{\boldsymbol{\theta}}_{\mathrm{NW}} = \frac{\sum_{i=1}^{N} \boldsymbol{\theta}^{(i)} k(\mathbf{y}^{(i)}, \mathbf{d})}{\sum_{i=1}^{N} k(\mathbf{y}^{(i)}, \mathbf{d})} \tag{33}$$

and make response predictions by setting $g(\boldsymbol{\theta}) = \tilde{\mathbf{y}}(\boldsymbol{\theta})$,

$$\hat{\boldsymbol{y}}_{\mathrm{NW}} = \frac{\sum_{i=1}^{N} \tilde{\mathbf{y}}^{(i)} k(\mathbf{y}^{(i)}, \mathbf{d})}{\sum_{i=1}^{N} k_{\kappa}(\mathbf{y}^{(i)}, \mathbf{d})} \tag{34}$$

where, now $\tilde{\mathbf{y}}^{(i)}$ is the prediction from the model $\boldsymbol{\theta}^{(i)}$. If the response to the same excitation which yielded $\mathbf{d}$ is to be computed then $\tilde{\mathbf{y}} = \mathbf{y}$. In a similar vein, Eq. (33) can also be extended to obtain an estimate to any function of $\boldsymbol{\theta}$.

The ability to make predictions using the correct model class is implicit in the kernel regression approach using kernels k_{ES} or k_{EB}. When the kernel k_{ES} or k_{EB} is used, then due to fact that these kernels have compact support, some of the drawn samples of $\boldsymbol{\theta}$ will carry no weight; i.e., $k(\mathbf{y}^{(i)}, \mathbf{d})$ will be zero for those $\boldsymbol{\theta}^{(i)}$ that are falsified for a given target identification probability ϕ. These realizations can be disregarded and sampling continues up until all the realizations have non-zero weights. This will automatically disregard model classes that are inconsistent with the observed data. We also note that similar computations can be performed when kernel regression is performed with k_{L} if a compact support is assigned in a manner similar to Eq. (13). Thus, similar to model falsified GABC, kernel regression is another way in which the degree of similarity between model predictions and measured data can be utilized, which leads to improved predictions, as we will show. However, the computational costs of kernel regression will be similar to those of model falsified ABC using the corresponding falsifier.

Parameter estimation using kernels based on model falsifiers

Table 11 shows the relative error in the Nadaraya-Watson estimates for the parameters of the base isolated structure described in Section 6 when $\phi = 0.99$ (the actual parameter estimates are provided in Table SM5 in the Supplemental Material and in (Dasgupta 2023)). The estimates are made using a sample of size 5000. Note that all model classes except the true Bouc-Wen model class ($\mathcal{M}_2$) are falsified for $\phi = 0.99$ as shown previously in Fig. 17. For the kernel k_{L}, only the model class $\mathcal{M}_2$ is considered because we did not assign it a compact support. The quality of the parameter estimates is very close to those obtained from the ABC posterior; the relative errors are very similar to those in Table 7, where we had used $\phi = 0.90$. The computational cost of performing kernel regression is the same as model falsified ABC with the corresponding kernels with the same value of ϕ. Although the parameter estimates obtained using model falsified GABC are better, note that it is more computationally expensive.

Response prediction using kernels based on model falsifiers

The response of the base isolated system described in Section 6 to the El Centro earthquake (the same excitation for which the measurements are available) and the Ridgrecrest earthquake (an alternate excitation) can be computed using kernel regression. Table 12 shows the normalized (with respect to the true response) RMSE of the predicted base acceleration and maximum of the absolute base acceleration. (Figs. SM8a and SM8b in the Supplemental Material, which can also be found in (Dasgupta 2023), show the Nadaraya-Watson estimate for the absolute acceleration at the base of the structure where it is clear that the estimates are in good agreement with the true response.) The results indicate good generalizability of the Nadaraya-Watson estimator.

IMPLICATIONS OF THIS WORK AND FUTURE RESEARCH DIRECTIONS

The main purpose of this work was to provide a Bayesian perspective on model falsification. Our reinterpretation will allow the results from model falsification to be viewed in a different light, primarily, unfalsified models are realizations of an approximate posterior density, and predictions and estimates obtained using the unfalsified models are posterior predictive quantities. In the process, we have also introduced model falsified (G)ABC wherein model falsifiers are appropriately adapted within (G)ABC frameworks.

Our reinterpretation also means that many of the desirable properties enjoyed by ABC can now be attributed to model falsification. Chief among them is perhaps the fact that model falsification may now be deemed to honor the principle of Occam's razor; therefore, falsification may implicitly favor simpler or parsimonious hypotheses, although that remains to be verified. Also, it may now be possible to perform *a posteriori* model validation using Bayesian statistical tools like posterior predictive checks and credible intervals. Model checking is a necessary and crucial step that should be conducted when carrying out inference (Gelman and Shalizi 2013) and, to the best of our knowledge, no such validation metrics have been developed for model falsification. Much of the ABC machinery, such as computationally efficient algorithms for sampling, can also be applied to reduce the computational burden of model falsification, much like we have used SMC.

Going the opposite direction, using model falsifiers as discrepancy measures means that ABC may be calibrated based on the frequentist properties of the falsifiers. As such, future work needs to investigate the automatic selection of ϕ such that any estimates obtained using model falsified ABC are consistent; see (Fearnhead and Prangle 2012; Ratmann et al. 2013) for related work. Model falsifiers could also take into consideration model errors by accounting for it in $\pi_{E_i}(e_i)$ (Goulet and Smith 2013b; Pai and Smith 2017; Pai et al. 2018). Therefore, the application of model falsified ABC to inference problems where the data generating model $\pi(\boldsymbol{y}|\boldsymbol{\theta})$ is misspecified or only partially known may be another interesting avenue of future research.

Another direction for future research could be the application of model falsification to summary statistics. Note that the approximation in ABC stems from two sources: first, from using the acceptance criteria in Eq. (3) with a looser tolerance, which is considered in this work; second, approximation can also be induced from using summary statistics, which are often not sufficient, particularly when dealing with high dimensional data such as time series data (for example, modal frequency and mode shape data, extracted from structural response, is routinely used for structural system identification or health monitoring (Yuen 2010)). The introduction of summary statistics can further boost the computational efficiency of model falsified ABC. We intend to explore model falsified (G)ABC with summary statistics in a future work.

CONCLUSIONS AND OUTLOOK

We have shown that model falsification is similar to approximate Bayesian computation. A new framework for ABC and generalized ABC that utilizes model falsifiers as discrepancy metrics and density kernels, respectively, has been introduced. We have also considered different types of error and likelihood domain falsifiers. Model falsified (G)ABC was applied to different inference tasks. The results show that inference using model falsified (G)ABC is satisfactory. The inferred parameters were found to agree with the true values and could generalize well. The results also indicate that model falsified (G)ABC may be a computationally efficient inference approach, compared to Bayesian inference, when the prior is non-informative. We have also shown how falsifier based kernels can be used for kernel regression to estimate parameters and/or make predictions via Nadaraya-Watson estimators.

DATA AVAILABILITY STATEMENT

The data, models, or code that support the findings of this study are available from the corresponding author upon reasonable request with the exception of the El Centro and Ridgecrest earthquake records, which can be obtained from (Center for Engineering Strong Motion Data 2019; Strong Motion Virtual Data Center 2019), and the open source `pyABC` toolbox (Klinger et al. 2018).

ACKNOWLEDGMENTS

The authors gratefully acknowledge the support of this work by the National Science Foundation through award CMMI 16-63667. The first author also acknowledges support from the University of Southern California through a Provost's Ph.D. Fellowship. Any opinions, findings, and conclusions or recommendations expressed in this material are those of the authors and do not necessarily reflect the views of NSF or USC. The authors also acknowledge the Center for Advanced Research Computing (CARC, carc.usc.edu) at the University of Southern California for providing computing resources that have contributed to the research results reported within this publication. The authors further acknowledge accessing strong-motion data through the Center for Engineering Strong Motion Data (CESMD), last visited on 17 November 2021; the networks or agencies providing the data used in this report are the California Strong Motion Instrumentation Program (CSMIP) and the USGS National Strong Motion Project (NSMP).

APPENDIX I. ALGORITHMS FOR APPROXIMATE BAYESIAN COMPUTATION

Algorithms 1 and 2, shown in Figs. 20 and 21, are the rejection based samplers used for performing ABC and generalized ABC, respectively. Both algorithms can be found in (Sisson et al. 2018, Chapter 1).

APPENDIX II. COMPUTATIONAL ASPECTS FOR IMPLEMENTING MODEL FALSIFIED (G)ABC

We highlight here some computational aspects regarding the implementation of model falsified ABC. First, all computation should be carried out in logarithmic scale. This not only helps with better conditioning of computations in the likelihood domain but also helps with the computation of probability densities and cumulative distribution functions (cdfs). For example, the successful implementation of ABC with falsifiers often required the computation of the standard normal cdf at very large negative values of the variate. These computations must be carried out in logarithmic scale using appropriate approximations, else all p-values in Eq. (8) will evaluate to zero. For instance, the standard normal cdf's logarithm is approximated using the `logphi` function available as part of the GPML toolbox (Rasmussen and Nickisch 2016) in MATLAB (The Mathworks, Inc. 2021), and the `scipy.norm` module (Virtanen et al. 2020) in Python (Van Rossum and Drake 2009). Moreover, when working with error domain falsifiers, it can be easier to implement the acceptance step within ABC as follows:

$$\max_{i=1,\ldots,N_m} -\log \tilde{p}_i \leq \kappa', \tag{35}$$

where $\kappa' = -\log(1 - \phi^{1/N_\mathrm{m}})$ and $-\log(1 - \phi)$ for falsifiers f_ES and f_EB, respectively. Similarly, instead of Eqs. (9) and (11), the acceptance step for the likelihood domain falsifiers can be modified as

$$-\sum_{i=1}^{N_m} \log \pi_{E_i}(\epsilon_i) \leq -\sum_{i=1}^{N_m} \min_{\underline{\epsilon}_i \leq e_i \leq \bar{\epsilon}_i} \log \pi_{E_i}(e_i) \tag{36}$$

and the error bounds $\underline{\epsilon}_i$ and $\bar{\epsilon}_i$ are derived as described previously.

APPENDIX III. ABC USING SEQUENTIAL MONTE CARLO METHODS

The SMC algorithm (Toni et al. 2009) used in the numerical examples shown in Sections 5 and 6 are implemented using the `pyABC` toolbox (Klinger et al. 2018); its basic algorithm is provided in Fig. 22. The SMC algorithm begins with N particles that are drawn from the parameter priors; subsequently, the particles explore the parameter space through repeated updates, ultimately providing a Monte Carlo approximation to the ABC posterior through the weights

$$w_t^{(i)} = \begin{cases} 1, & \text{if } t = 0 \\ \pi(\boldsymbol{\theta}^* | \mathcal{M}_t^{(i)}) \Big/ \left[\sum_{j=1}^{N} w_{t-1}^{(j)} K_{p,t} \left(\boldsymbol{\theta}^* | \boldsymbol{\theta}_{t-1}^{(j)} \right) \right], & \text{if } t > 0 \end{cases} \tag{37}$$

The outputs of Algorithm 3 can be used to compute the posterior model class probabilities as follows

$$P_{\text{ABC}}(\mathcal{M}_k | \mathbf{d}) = \frac{1}{N} \sum_{j=1}^{N} \mathbb{I}[\mathcal{M}^{(j)} = \mathcal{M}_k] \tag{38}$$

Further, Algorithm 3 reverts to Algorithm 1 when $K = 1$ and $N_t = 1$.

Several improvements over the standard SMC approach have also been proposed; we note only those that we utilize. The thresholds κ_t and the number of iterations N_t can be adaptively selected (Beaumont et al. 2009; Del Moral et al. 2012), which helps improve the conditioning of acceptance rates, ultimately increasing sampling efficiency. In the parameter estimation example from Section 5, the threshold κ_t at iteration t is chosen such that τN particles are retained, with $\tau = 0.5$. Moreover, the perturbation kernel $K_{p,t}$ for the t^{th} population can also be adaptively designed; throughout this work, we have perturbed the particles in every population using a multivariate normal density kernel whose precision matrix is adaptively determined (see the documentation for the `pyABC` toolbox (Klinger et al. 2018) for details).

To perform GABC with the density kernel k, the acceptance criteria in Step 15 of Algorithm 3 is modified as follows (Schälte and Hasenauer 2020)

$$\text{Accept } \boldsymbol{\theta}^*, \mathcal{M}^* \text{ with probability } \min\left\{1, \frac{k(\mathbf{y}^*, \mathbf{d})}{C}\right\}, \tag{39}$$

where k is the kernel being used, and C is a normalization constant such that $C \geq \max_{\mathbf{y}} k(\mathbf{y}, \mathbf{d})$. Choosing the normalization constant C is critical to the performance of the GABC approach using SMC. If C is too small, relative to the realized values of $k(\mathbf{y}, \mathbf{d})$, then all of the models are accepted. On the other hand, if C is too large, then the acceptance rates drop, making the approach computationally inefficient. As a remedy, Schälte and Hasenauer (2020) proposed an efficient scheme that further modifies the acceptance criteria from Eq. (39) to

$$\text{Accept } \boldsymbol{\theta}^*, \mathcal{M}^* \text{ with probability } \min\left\{1, \left(\frac{k(\mathbf{y}^*, \mathbf{d})}{C_t}\right)^{1/T_t}\right\} \tag{40}$$

where C_t and T_t are the normalization constant and temperature at population t, respectively. To ensure that the samples indeed belong to the approximate posterior, $T_1 > T_2 > \ldots > T_{N_t} = 1$ is used and the weights are accordingly modified as follows

$$\bar{w}_t^{(i)} \propto \frac{k(\mathbf{y}^*, \mathbf{d})^{1/T_t}}{\min\left\{1, [k(\mathbf{y}^*, \mathbf{d})/C_t]^{1/T_t}\right\}} \cdot \frac{\pi(\boldsymbol{\theta}^{(i)} | \mathcal{M}_t^{(i)})}{w_t^{(i)}} \tag{41}$$

where $w_t^{(i)}$ can be obtained using Eq. (37). Schälte and Hasenauer (2020) also proposed multiple approaches for decaying the temperatures, among which is a scheme, used in all examples studied herein, that aims to maintain the target acceptance rate at a predefined level. As an example, the temperatures at different population levels and the corresponding acceptance probabilities across different model classes for the base isolated structure in Section 6 are shown in Figs. 23a and 23b, respectively. As the population evolves in the modified SMC algorithm, the temperature is gradually reduced to 1 such that all particles belong to the approximate posterior.

APPENDIX IV. SUPPLEMENTAL MATERIAL

Sections SM1–SM5, including Figs. SM1–SM8 and Tables SM1–SM5, are available online in the ASCE Library (ascelibrary.org) as a companion to this paper.

REFERENCES

Abdessalem, A. B., Dervilis, N., Wagg, D., and Worden, K. (2018). “Model selection and parameter estimation in structural dynamics using approximate Bayesian computation.” *Mechanical Systems and Signal Processing*, 99, 306–325.

Abdessalem, A. B., Dervilis, N., Wagg, D., and Worden, K. (2019). “Model selection and parameter estimation of dynamical systems using a novel variant of approximate Bayesian computation.” *Mechanical Systems and Signal Processing*, 122, 364–386.

Abdi, H. (2007). “Bonferroni and Šidák corrections for multiple comparisons.” *Encyclopedia of Measurement and Statistics*, 3, 103–107.

Barber, S., Voss, J., and Webster, M. (2015). “The rate of convergence for approximate Bayesian computation.” *Electronic Journal of Statistics*, 9(1), 80–105.

Barros, J., Chiachío, M., Chiachío, J., and Cabanilla, F. (2022). “Adaptive approximate Bayesian computation by subset simulation for structural model calibration.” *Computer-Aided Civil and Infrastructure Engineering*, 37(6), 726–745.

Beaumont, M. A., Cornuet, J.-M., Marin, J.-M., and Robert, C. P. (2009). “Adaptive approximate Bayesian computation.” *Biometrika*, 96(4), 983–990.

Beaumont, M. A., Zhang, W., and Balding, D. J. (2002). “Approximate Bayesian computation in population genetics.” *Genetics*, 162(4), 2025–2035.

Benjamini, Y. and Hochberg, Y. (1995). “Controlling the false discovery rate: a practical and powerful approach to multiple testing.” *Journal of the Royal statistical society: Series B (Methodological)*, 57(1), 289–300.

Beven, K. J. (1993). “Prophecy, reality and uncertainty in distributed hydrological modelling.” *Advances in Water Resources*, 16(1), 41–51.

Beven, K. J. (2011). *Rainfall-runoff modelling: the primer*. John Wiley & Sons.

Beven, K. J. and Freer, J. (2001). “Equifinality, data assimilation, and uncertainty estimation in mechanistic modelling of complex environmental systems using the GLUE methodology.” *Journal of Hydrology*, 249(1-4), 11–29.

Blum, M. G. (2010). "Approximate Bayesian computation: A nonparametric perspective." *Journal of the American Statistical Association*, 105(491), 1178–1187.

Center for Engineering Strong Motion Data (2019). https://www.strongmotioncenter.org/cgi-bin/CESMD/stationhtml.pl?stationID=CITOW2&network=SCSN. Accessed: 2021-11-17.

Chiachio, M., Beck, J. L., Chiachio, J., and Rus, G. (2014). "Approximate Bayesian computation by subset simulation." *SIAM Journal on Scientific Computing*, 36(3), A1339–A1358.

Dasgupta, A. (2023). "Model falsification: new insights, methods and applications." Ph.D. thesis, University of Southern California, Los Angeles, California, USA.

Dasgupta, A. and Johnson, E. A. (2022). "Model falsification from a bayesian viewpoint with applications to system identification and model selection." *8th World Conference on Structural Control and Monitoring (8WCSCM)*. in press.

De, S., Brewick, P. T., Johnson, E. A., and Wojtkiewicz, S. F. (2018). "Investigation of model falsification using error and likelihood bounds with application to a structural system." *Journal of Engineering Mechanics*, 144(9), 04018078.

Del Moral, P., Doucet, A., and Jasra, A. (2012). "An adaptive sequential Monte Carlo method for approximate Bayesian computation." *Statistics and Computing*, 22(5), 1009–1020.

Durrett, R. (2019). *Probability: Theory and Examples*. Cambridge University Press, 4^{th} edition.

Elías-Zúñiga, A. (2013). "Exact solution of the cubic-quintic Duffing oscillator." *Applied Mathematical Modelling*, 37(4), 2574–2579.

Evans, S. N. and Stark, P. B. (2002). "Inverse problems as statistics." *Inverse Problems*, 18(4), R55.

Fang, S.-E., Chen, S., Lin, Y.-Q., and Dong, Z.-L. (2019). "Probabilistic damage identification incorporating approximate Bayesian computation with stochastic response surface." *Mechanical Systems and Signal Processing*, 128, 229–243.

Fearnhead, P. and Prangle, D. (2012). "Constructing summary statistics for approximate Bayesian computation: semi-automatic approximate Bayesian computation." *Journal of the Royal Statistical Society: Series B (Statistical Methodology)*, 74(3), 419–474.

Freedman, D. (1997). "Some issues in the foundation of statistics." *Topics in the Foundation of Statistics*, Springer, 19–39.

Freedman, D. A. and Stark, P. B. (2003). "What is the chance of an earthquake?." *NATO Science Series IV: Earth and Environmental Sciences*, 32, 201–213.

Gelman, A. and Shalizi, C. R. (2013). "Philosophy and the practice of Bayesian statistics." *British Journal of Mathematical and Statistical Psychology*, 66(1), 8–38.

Goulet, J.-A., Coutu, S., and Smith, I. F. (2013). "Model falsification diagnosis and sensor placement for leak detection in pressurized pipe networks." *Advanced Engineering Informatics*, 27(2), 261–269.

Goulet, J.-A., Kripakaran, P., and Smith, I. F. (2010). "Multimodel structural performance monitoring." *Journal of Structural Engineering*, 136(10), 1309–1318.

Goulet, J.-A. and Smith, I. F. (2013a). "Performance-driven measurement system design for structural identification." *Journal of Computing in Civil Engineering*, 27(4), 427–436.

Goulet, J.-A. and Smith, I. F. (2013b). "Structural identification with systematic errors and unknown uncertainty dependencies." *Computers & Structures*, 128, 251–258.

Hazra, I. and Pandey, M. D. (2021). "A likelihood-free approach towards Bayesian modeling of degradation growths using mixed-effects regression." *Computers & Structures*, 244, 106427.

Hazra, I., Pandey, M. D., and Manzana, N. (2020). "Approximate Bayesian computation (ABC) method for estimating parameters of the gamma process using noisy data." *Reliability Engineering & System Safety*, 198, 106780.

Hwang, J. and Chiou, J. (1996). "An equivalent linear model of lead-rubber seismic isolation bearings." *Engineering Structures*, 18(7), 528–536.

Klinger, E., Rickert, D., and Hasenauer, J. (2018). "pyABC: Distributed, likelihood-free inference." *Bioinformatics*, 34(20), 3591–3593.

Kroese, D. P., Taimre, T., and Botev, Z. I. (2013). *Handbook of Monte Carlo methods*, Vol. 706. John Wiley & Sons.

Milne, P. (1995). "A Bayesian defence of Popperian science?." *Analysis*, 55(3), 213–215.

Moser, G., Paal, S. G., and Smith, I. F. (2018). “Leak detection of water supply networks using error-domain model falsification.” *Journal of Computing in Civil Engineering*, 32(2), 04017077.

Pai, S. G., Nussbaumer, A., and Smith, I. F. (2018). “Comparing structural identification methodologies for fatigue life prediction of a highway bridge.” *Frontiers in Built Environment*, 3, 73.

Pai, S. G. and Smith, I. F. (2017). “Comparing three methodologies for system identification and prediction.” *14th International Probabilistic Workshop*, Springer, 81–95.

Pasquier, R. and Smith, I. F. (2015). “Robust system identification and model predictions in the presence of systematic uncertainty.” *Advanced Engineering Informatics*, 29(4), 1096–1109.

Pritchard, J. K., Seielstad, M. T., Perez-Lezaun, A., and Feldman, M. W. (1999). “Population growth of human Y chromosomes: a study of Y chromosome microsatellites.” *Molecular Biology and Evolution*, 16(12), 1791–1798.

Ramallo, J. C., Johnson, E. A., and Spencer, Jr, B. F. (2002). ““Smart” base isolation systems.” *Journal of Engineering Mechanics*, 128(10), 1088–1099.

Rasmussen, C. E. and Nickisch, H. (2016). “The GPML Toolbox version 4.0.” *Technical Documentation*.

Ratmann, O., Camacho, A., Meijer, A., and Donker, G. (2013). “Statistical modelling of summary values leads to accurate approximate Bayesian computations.” *arXiv preprint arXiv:1305.4283*.

Rosenkrantz, R. D. (1977). “Bayes and Popper.” *Inference, Method and Decision*, Springer, 118–134.

Rubin, D. B. (1984). “Bayesianly justifiable and relevant frequency calculations for the applied statistician.” *The Annals of Statistics*, 1151–1172.

Sadegh, M. and Vrugt, J. (2013). “Bridging the gap between GLUE and formal statistical approaches: approximate Bayesian computation.” *Hydrology and Earth System Sciences*, 17(12), 4831–4850.

Schälte, Y. and Hasenauer, J. (2020). “Efficient exact inference for dynamical systems with noisy measurements using sequential approximate Bayesian computation.” *Bioinformatics*, 36, i551–i559.

Sisson, S. A., Fan, Y., and Beaumont, M. (2018). *Handbook of approximate Bayesian computation*. CRC Press.

Stark, P. B. and Tenorio, L. (2010). "A primer of frequentist and Bayesian inference in inverse problems." *Large–Scale Inverse Problems and Quantification of Uncertainty*, John Wiley & Sons, Ltd, Chapter 2, 9–32.

Strong Motion Virtual Data Center (2019). https://www.strongmotioncenter.org/vdc/scripts/plot.plx?stn=6030&evt=1350. Accessed: 2021-11-17.

Tavaré, S., Balding, D. J., Griffiths, R. C., and Donnelly, P. (1997). "Inferring coalescence times from DNA sequence data." *Genetics*, 145(2), 505–518.

The Mathworks, Inc. (2021). *MATLAB version 9.10.0.1739362 (R2021a)*. Natick, Massachusetts.

Toni, T., Welch, D., Strelkowa, N., Ipsen, A., and Stumpf, M. P. (2009). "Approximate Bayesian computation scheme for parameter inference and model selection in dynamical systems." *Journal of the Royal Society Interface*, 6(31), 187–202.

Vakilzadeh, M. K., Huang, Y., Beck, J. L., and Abrahamsson, T. (2017). "Approximate Bayesian computation by subset simulation using hierarchical state-space models." *Mechanical Systems and Signal Processing*, 84, 2–20.

Van Rossum, G. and Drake, F. L. (2009). *Python 3 Reference Manual*. CreateSpace, Scotts Valley, CA.

Virtanen, P., Gommers, R., Oliphant, T. E., Haberland, M., Reddy, T., Cournapeau, D., Burovski, E., Peterson, P., Weckesser, W., Bright, J., van der Walt, S. J., Brett, M., Wilson, J., Millman, K. J., Mayorov, N., Nelson, A. R. J., Jones, E., Kern, R., Larson, E., Carey, C. J., Polat, İ., Feng, Y., Moore, E. W., VanderPlas, J., Laxalde, D., Perktold, J., Cimrman, R., Henriksen, I., Quintero, E. A., Harris, C. R., Archibald, A. M., Ribeiro, A. H., Pedregosa, F., van Mulbregt, P., and SciPy 1.0 Contributors (2020). "SciPy 1.0: Fundamental Algorithms for Scientific Computing in Python." *Nature Methods*, 17, 261–272.

Vrugt, J. A. and Sadegh, M. (2013). "Toward diagnostic model calibration and evaluation: Approximate Bayesian computation." *Water Resources Research*, 49(7), 4335–4345.

Wasserman, L. (2006). *All of nonparametric statistics*. Springer Science & Business Media.

Wen, Y.-K. (1976). "Method for random vibration of hysteretic systems." *Journal of the Engineering Mechanics Division*, 102(2), 249–263.

Wilkinson, R. (2014). "Accelerating ABC methods using Gaussian processes." *Artificial Intelligence and Statistics*, Proceedings of Machine Learning Research, 1015–1023.

Wilkinson, R. D. (2013). "Approximate Bayesian computation (ABC) gives exact results under the assumption of model error." *Statistical applications in genetics and molecular biology*, 12(2), 129–141.

Yuen, K.-V. (2010). *Bayesian methods for structural dynamics and civil engineering*. John Wiley & Sons.

List of Tables

TABLE 1: Scale factors, significance levels and thresholds for different model falsification approaches and error control control criterion. ϕ is the specified target identification probability, and N_m is the number of measurements

Error control	Error domain (ED)			Likelihood domain (LD)		
	Notation	r_i	κ	Notation	α_i	κ
FWER/Šidák	f_{ES}	1	$\phi^{1/N_{\mathrm{m}}}$	f_{LS}	$1-\phi^{1/N_{\mathrm{m}}}$	Eq. (11)
FDR/BH	f_{EB}	N_m/i	ϕ	f_{LB}	$(1-\phi)i/N_{\mathrm{m}}$	

TABLE 2: Relative error in the parameter estimates of the cubic-quintic system obtained using model falsified ABC with different model falsifiers and the associated COV (given in parentheses). The reported estimates are averages across ten independent runs

Parameter	Falsifier			
	f_{ES}	f_{ES}	f_{LS}	f_{LB}
m	0.012 (0.073)	0.014 (0.067)	0.039 (0.102)	0.009 (0.087)
c	0.819 (0.572)	0.612 (0.583)	1.198 (0.654)	1.072 (0.613)
k	0.020 (0.216)	0.023 (0.220)	0.110 (0.352)	0.106 (0.299)
k_3	0.668 (0.607)	0.662 (0.577)	1.535 (0.628)	1.113 (0.602)
k_5	0.083 (0.244)	0.097 (0.238)	0.081 (0.447)	0.082 (0.412)

TABLE 3: Comparison of the normalized RMSE of the predicted response from the model identified using model falsified ABC with different falsifiers, and the total number of model simulations necessary for the inference. The average across ten independent runs is reported

Falsifier	Normalized RMSE for different excitations		Total simulations
	Random Gaussian $w(t)$	Harmonic $\tilde{w}(t)$	
f_{ES}	0.001	0.001	2.47×10^6
f_{EB}	0.001	0.001	2.38×10^6
f_{LS}	0.003	0.004	1.66×10^5
f_{LB}	0.004	0.003	2.37×10^5

TABLE 4: Relative error in the parameter estimates of the cubic-quintic system obtained using model falsified GABC with different kernels and the associated COV (given in parenthesis). The reported estimates for kernel k_{ES} and k_{EB} are averages across ten independent runs.

Parameter	Kernel		
	k_{ES}	k_{ES}	k_{L}
m	0.006 (0.065)	0.003 (0.066)	0.024 (0.035)
c	0.676 (0.541)	0.660 (0.550)	0.185 (0.368)
k	0.023 (0.130)	0.031 (0.204)	0.020 (0.130)
k_3	0.463 (0.594)	0.565 (0.598)	0.644 (0.382)
k_5	0.096 (0.232)	0.107 (0.249)	0.133 (0.192)

TABLE 5: Comparison of the normalized RMSE of the predicted reponse from the posterior mean of the system parameters obtained from different kernels and the total number of model simulations necessary for the inference. The average across ten independent runs is reported for kernels k_{ES} and k_{EB}

Falsifier or Kernel	Normalized RMSE for different excitations		Total simulations
	Random Gaussian	Harmonic	
k_{ES}	0.001	0.001	5.34×10^7
k_{EB}	0.006	0.002	1.73×10^7
k_{L}	0.027	0.056	$> 10^8$

TABLE 6: Parameter priors for different model classes. Note that $X \sim \log\mathcal{N}(\mu, \sigma^2)$ means that the random variable X is log-normally distributed with mean μ and variance σ^2. Similarly, $X \sim \mathcal{U}(a, b)$ means that the random variable X is uniformly distributed between a and b

Parameter	True value	Prior
k_{post}	4.0 MN/m	$\log\mathcal{N}$(4.5,0.25) MN/m
c_{b}	20 KN·s/m^2	$\log\mathcal{N}$(20,4) KN·s/m^2
r_{k}	0.1667	$\mathcal{U}$(0.15, 0.17)
r_{d}	N/A	$\mathcal{U}$(2.0, 3.0)
Q_{y} (%mg)	5.00	$\mathcal{U}$(4.25, 5.25)

TABLE 7: Relative error of the posterior mean of the Bouc-Wen model class parameters, and the associated COV (given in parenthesis), obtained using model falsified ABC with different model falsifiers when $\phi = 0.90$

Parameter	Falsifier			
	f_{ES}	f_{ES}	f_{LS}	f_{LB}
k_{post} (MN/m)	0.082 (0.042)	0.082 (0.041)	0.106 (0.047)	0.100 (0.047)
c_{b} (kN·s/m)	0.247 (0.199)	0.246 (0.199)	0.251 (0.204)	0.250 (0.202)
r_{k}	0.026 (0.031)	0.024 (0.031)	0.032 (0.037)	0.032 (0.037)
Q_{y} ($\% mg$)	0.079 (0.047)	0.079 (0.049)	0.060 (0.059)	0.059 (0.060)

TABLE 8: Normalized RMSE between true response and the ABC posterior mean response for different falsifiers with $\phi = 0.90$. Note that the measured responses were from the El Centro earthquake

Falsifier	Absolute base acceleration		Absolute peak base acceleration	
	El Centro	Ridgecrest	El Centro	Ridgecrest
f_{ES}	0.115	0.202	0.035	0.048
f_{EB}	0.112	0.198	0.034	0.047
f_{LS}	0.150	0.248	0.045	0.047
f_{LB}	0.156	0.256	0.047	0.048

TABLE 9: Relative error of the posterior mean of the Bouc-Wen model class parameters, and the associated COV (given in parenthesis), obtained using model falsified GABC with different kernels

Parameter	Kernel		
	k_{ES}	k_{ES}	k_{L}
k_{post} (MN/m)	0.060 (0.036)	0.070 (0.040)	0.004 (0.015)
c_{b} (kN·s/m)	0.231 (0.207)	0.249 (0.196)	0.253 (0.191)
r_{k}	0.016 (0.024)	0.019 (0.031)	0.004 (0.012)
Q_{y} (%mg)	0.059 (0.042)	0.070 (0.047)	0.007 (0.008)

TABLE 10: Normalized RMSE between true response and the model falsified GABC approximate posterior predictive mean response for different falsifiers with $\phi = 0.99$. The measurements are recorded when the structure is excited by the El Centro earthquake excitation

Falsifier	Absolute Base acceleration		Peak absolute base acceleration	
	El Centro	Ridgecrest	El Centro	Ridgecrest
k_{ES}	0.084	0.154	0.025	0.034
k_B	0.095	0.172	0.029	0.040
k_L	0.008	0.008	0.002	0.002

TABLE 11: Relative error in the Nadaraya-Watson estimates of the parameters of the base isolated structure obtained using different kernels

Parameter	Kernel		
	k_{ES}	k_{ES}	k_{L}
k_{post} (MN/m)	0.096	0.078	0.124
c_{b} (kN·s/m)	0.239	0.248	0.244
r_{k}	0.035	0.025	0.041
Q_{y} (%mg)	0.085	0.077	0.046

TABLE 12: Normalized RMSE between true response and the Nadaraya-Watson estimator computed using different kernels. Note that measurements were recorded when the structure was excited using the El Centro earthquake

Falsifier	Base acceleration		Absolute peak base acceleration	
	El Centro	Ridgecrest	El Centro	Ridgecrest
k_{ES}	0.082	0.153	0.025	0.034
k_{EB}	0.093	0.174	0.028	0.041
k_{L}	0.007	0.007	0.001	1×10^{-4}

List of Figures

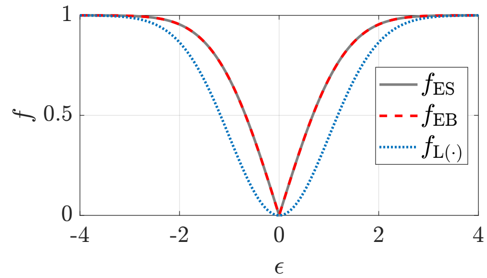

FIG. 1: Plot of different discrepancy metrics as functions of ϵ assuming $\epsilon \sim \mathcal{N}(0, 1)$

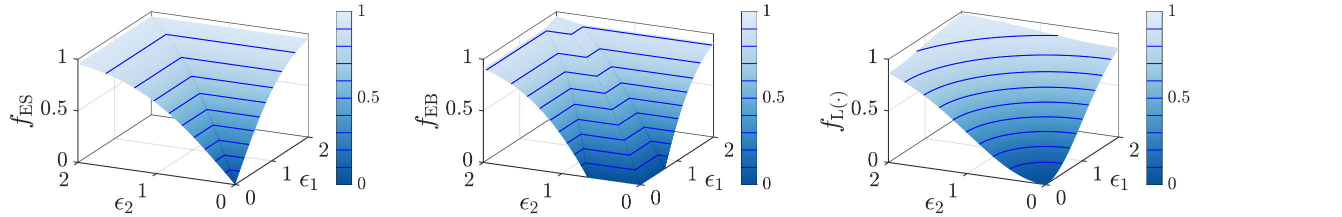

FIG. 2: Plot of different discrepancy metrics as functions of $\boldsymbol{\epsilon} = [\epsilon_1, \epsilon_2]^{\mathrm{T}}$ assuming $\epsilon_1, \epsilon_2 \sim \mathcal{N}(0, 1)$. Note that under Assumptions 1 and 2, as is the case here, $f_{\mathrm{LS}} = f_{\mathrm{LB}}$

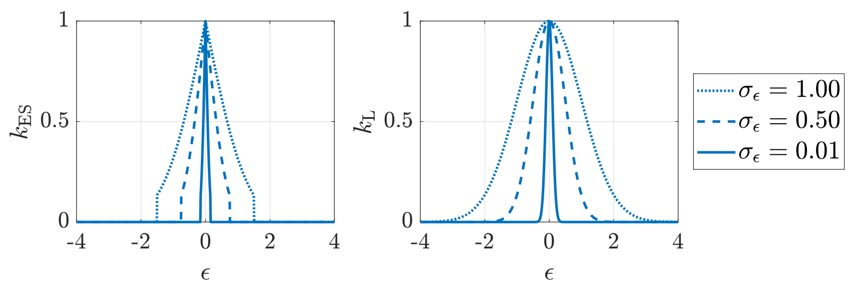

FIG. 3: Plot of different kernels as functions of ϵ in one dimension assuming $\epsilon \sim \mathcal{N}(0, \sigma_\epsilon)$ for $\sigma_\epsilon = 1, 0.5, 0.01$. The kernel $k_{\rm ES}$ is constrained to appropriate intervals which correspond to choosing $\phi = 0.90$

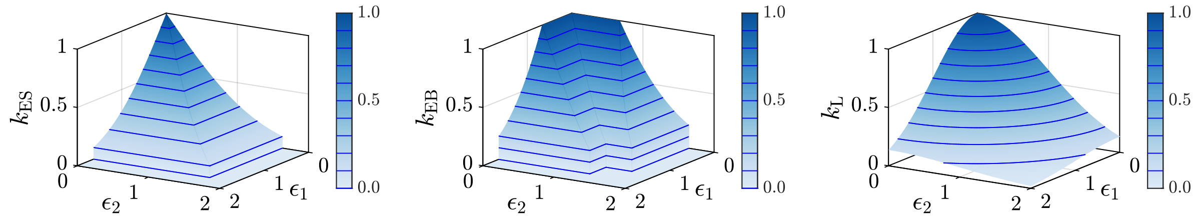

FIG. 4: Plot of different kernels as functions of $\boldsymbol{\epsilon} = [\epsilon_1, \epsilon_2]^{\mathrm{T}}$ in two dimensions assuming $\epsilon_1, \epsilon_2 \sim \mathcal{N}(0, 1)$. The kernels are appropriately constrained with $\phi = 0.90$

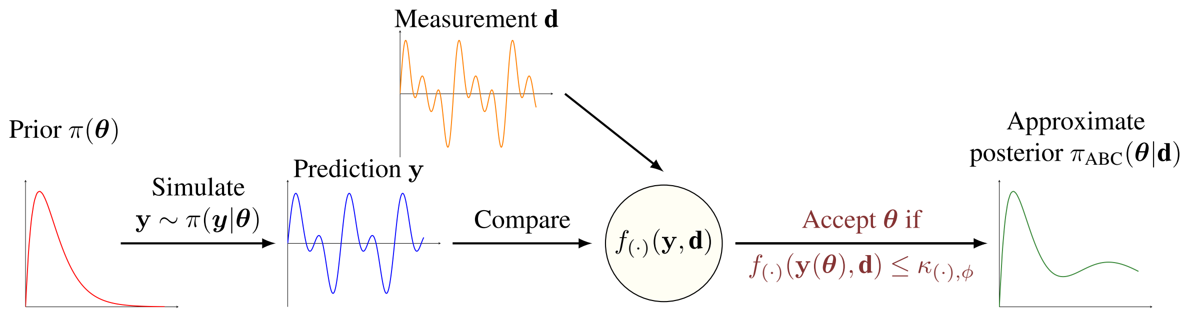

FIG. 5: Schematic of model falsified ABC

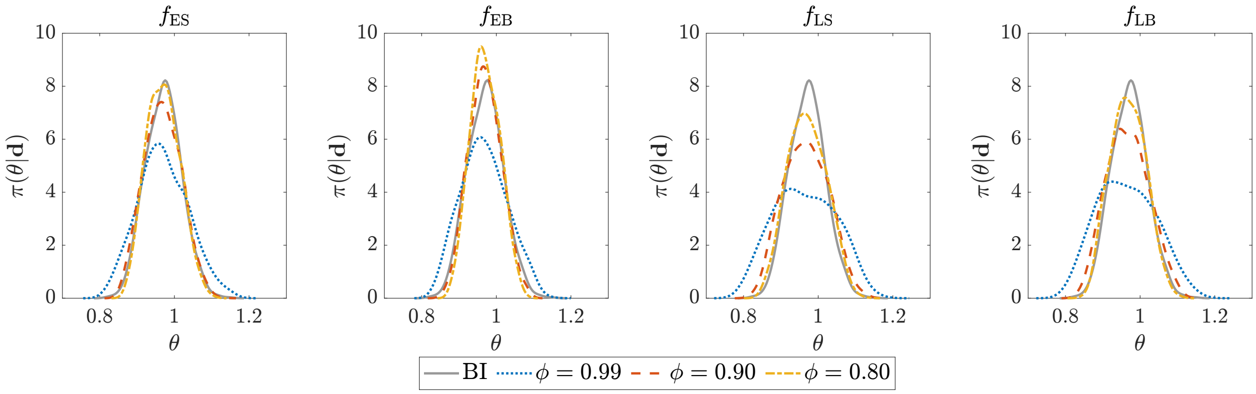

FIG. 6: Approximate posterior pdf of θ obtained from model falsified ABC performed using different falsifiers as the target identification probability ϕ is varied. BI = Bayesian Inference

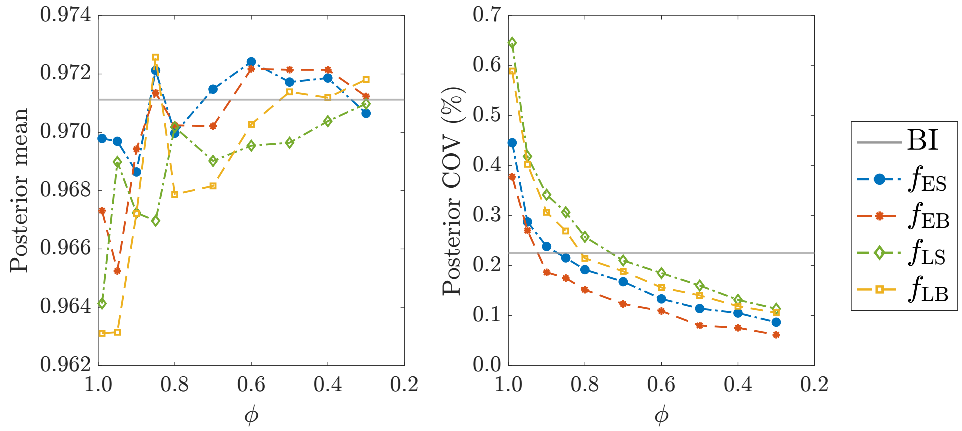

FIG. 7: Mean (left) and COV (right) of the approximate posterior pdf of θ obtained from model falsified ABC performed using different falsifiers as the target identification probability ϕ is varied. BI = Bayesian inference

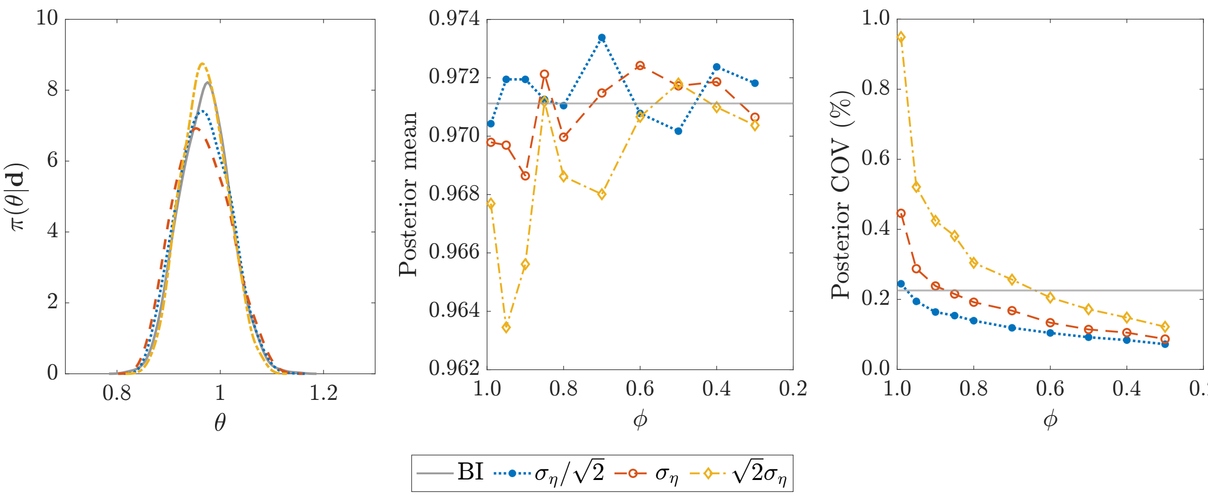

FIG. 8: Approximate posterior pdf of θ obtained using f_{ES} with target identification probability $\phi = 0.90$ and different values of the assumed variance of the residual errors σ_ϵ (left), and their respective mean (center) and COV (right). BI = Bayesian Inference

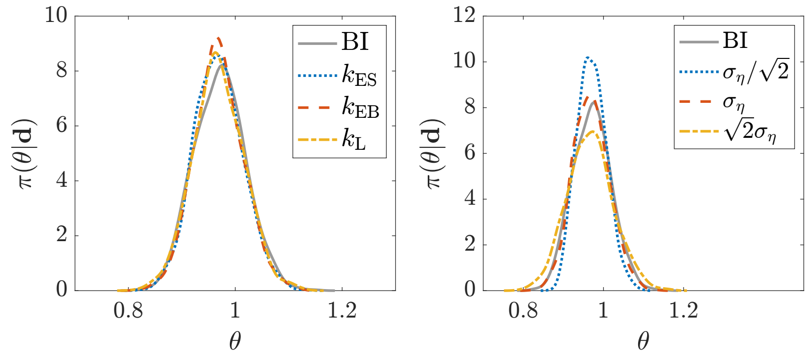

FIG. 9: Approximate posterior pdf of θ obtained from model falsified GABC performed using different falsifiers (left) and with kernel $k_{\rm ES}$ as σ_ϵ is varied (right). In this study we set $\phi = 0.99$. BI = Bayesian Inference

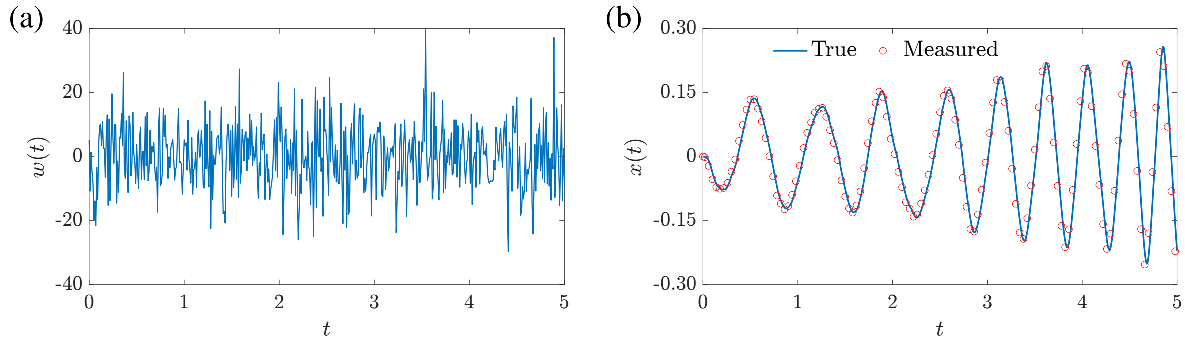

FIG. 10: (a) Forcing function $w(t)$ used to excite the cubic-quintic system; (b) True displacement and the measurements of the cubic-quintic system to be used for identification

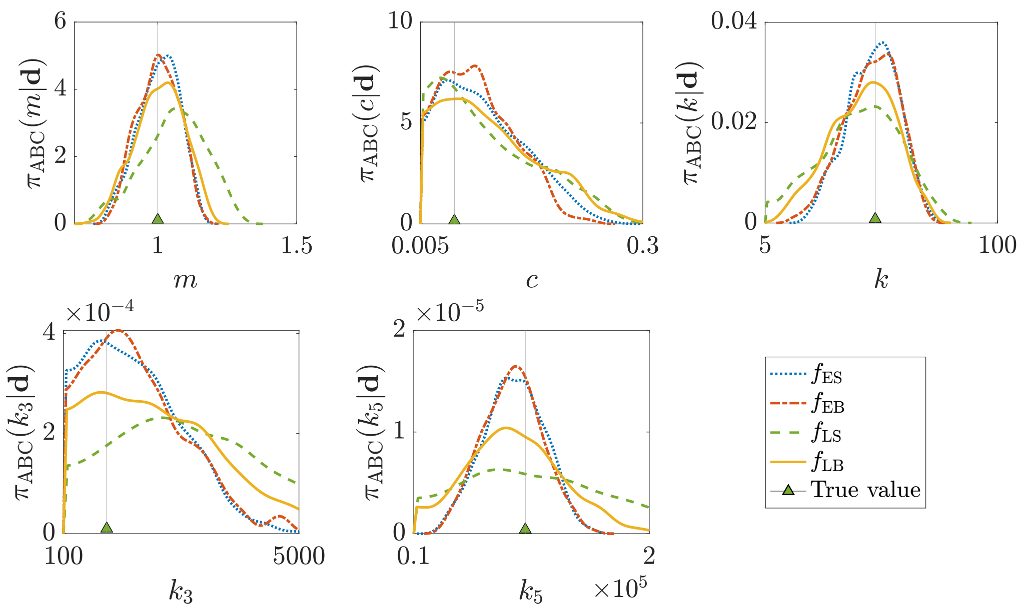

FIG. 11: Approximate posterior distribution of the cubic-quintic system's parameters obtained using model falsified ABC with different falsifiers

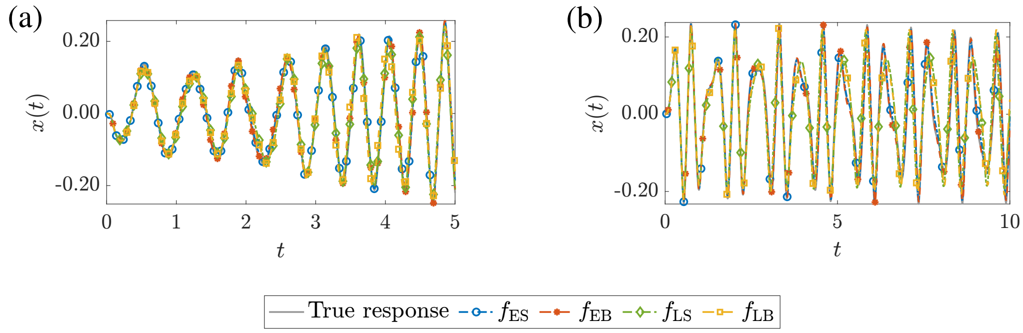

FIG. 12: Predicted response to (a) random Gaussian excitation $w(t)$ and (b) harmonic excitation $\tilde{w}(t)$ using the posterior mean of the parameter vector $\boldsymbol{\theta}$ of the cubic-quintic system estimated using model falsified ABC performed with different falsifiers

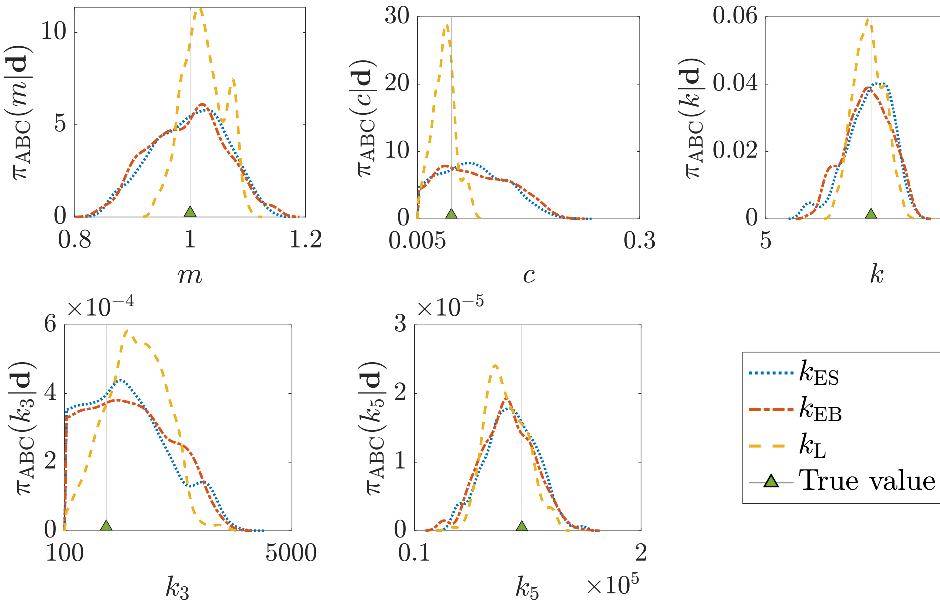

FIG. 13: Approximate posterior distribution of the cubic-quintic system's parameters obtained using model falsified GABC with different kernels

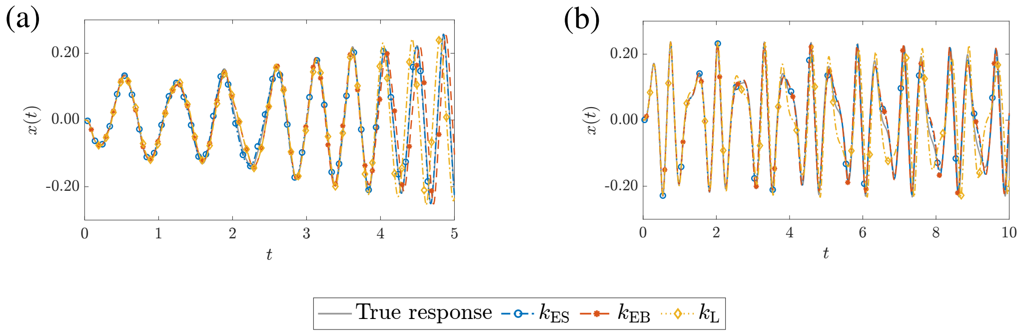

FIG. 14: Predicted response to (a) random Gaussian and (b) harmonic excitation from the approximate parameter posterior's mean of the cubic-quintic system estimated using different falsifiers used as a kernel for GABC

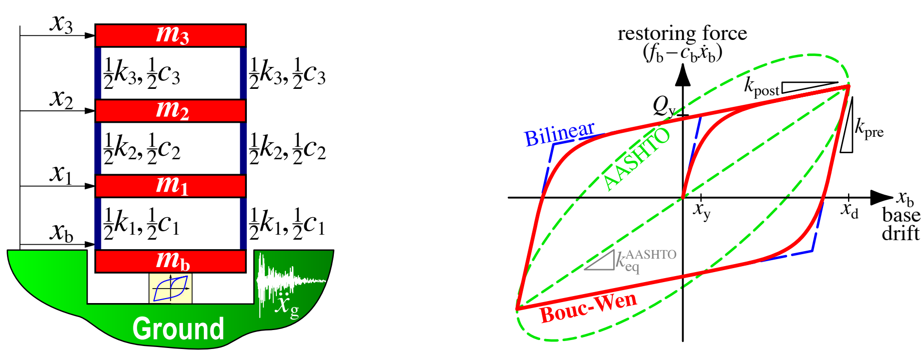

(a) (b)

FIG. 15: (a) Shear frame super-structure of the base isolated structure (b) Representative force displacement behavior of various model classes for the base isolation device. Both figures have been adapted from (De et al. 2018)

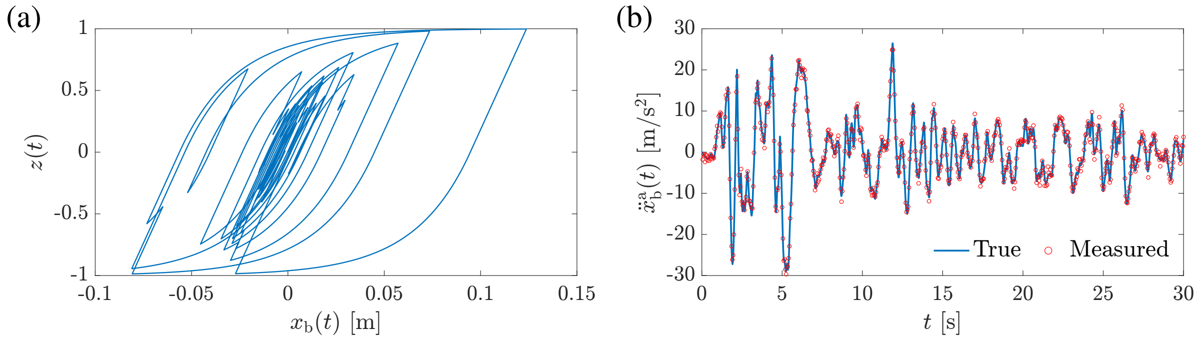

FIG. 16: Time histories of (a) the evolutionary variable $z(t)$ showing hysteretic behavior of the isolation layer and (b) the absolute base acceleration of the base isolated structure excited by the N–S El Centro ground motion

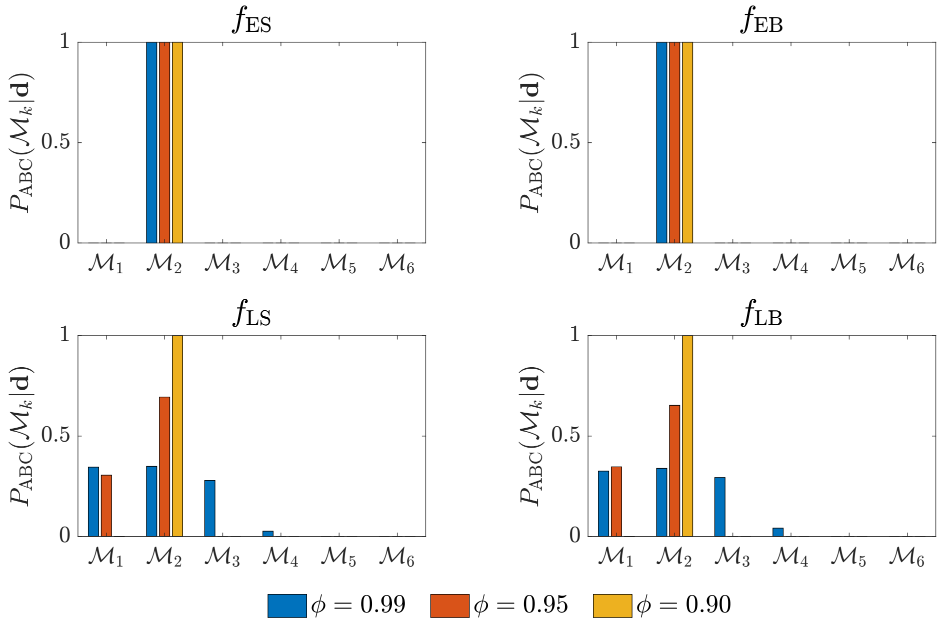

FIG. 17: Posterior model class probabilities using model falsified ABC with different falsifiers and target identification probabilities ϕ

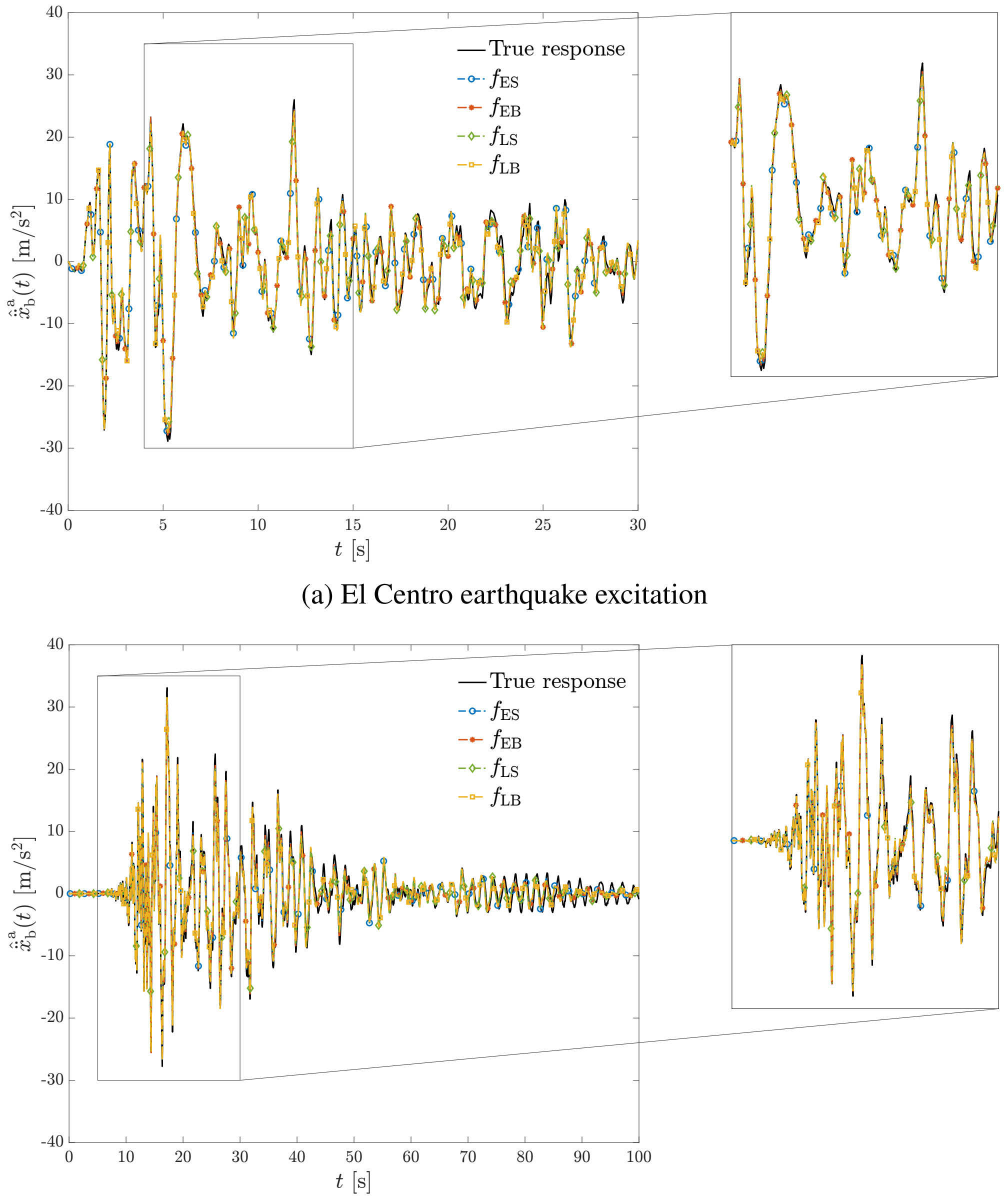

(a) El Centro earthquake excitation

(b) Ridgecrest earthquake excitation

FIG. 18: Approximate posterior predicted mean absolute base acceleration of the base isolated structure when subjected to (a) the El Centro earthquake and (b) the Ridgecrest earthquake base excitations from model falsified ABC with different falsifiers and when the measurements were recorded from the El Centro-excited structure

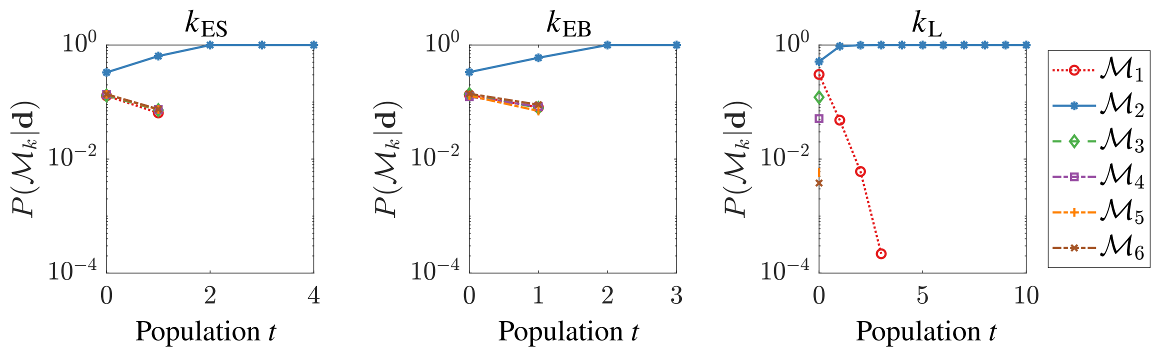

FIG. 19: Posterior model class probabilities of model classes at different populations t in the GABC approach for different kernels

Input: N : number of samples required, κ : threshold

for $t = 1$ to N **do**

  repeat

    Generate candidate model $\boldsymbol{\theta}'$ from prior distribution $\pi(\boldsymbol{\theta})$;

    Simulate candidate model prediction realization $\mathbf{y}'$ from $\pi(\boldsymbol{y}|\boldsymbol{\theta}')$;

  until $\rho(\mathbf{y}', \mathbf{d}) \leq \kappa$;

  Set $(\boldsymbol{\theta}^{(t)}, \mathbf{y}^{(t)})$ as $(\boldsymbol{\theta}', \mathbf{y}')$;

end

Output: $\boldsymbol{\theta}^{(1)}, \boldsymbol{\theta}^{(2)}, \ldots, \boldsymbol{\theta}^{(N)}$, which are realizations from $\pi_{\text{ABC}}(\boldsymbol{\theta}|\mathbf{d})$

FIG. 20: Algorithm 1: Likelihood free rejection sampler for standard ABC

```
   Input: N : number of samples required, k : kernel function, C ≥ max_y k(y, d)
1  for t = 1 to N do
2      Generate candidate model θ′ from prior distribution π(θ) ;
3      Simulate candidate model prediction realization y′ from π(y|θ′) ;
4      Draw u ~ 𝒰(0, 1) ;
5      if u ≤ k(y′, d)/C then set (θ^(t), y^(t)) as (θ′, y′);
6      else Go to Step 2 ;
7  end
   Output: θ^(1), θ^(2), ..., θ^(N), which are realizations from π_GABC(θ|d)
```

FIG. 21: Algorithm 2: Likelihood free rejection sampler for generalized ABC

Input: $\mathscr{M} = \{\mathcal{M}_1, \mathcal{M}_2, \ldots, \mathcal{M}_K\}$: K competing model classes
$P(\mathcal{M}_k)$: model class priors
$\pi(\boldsymbol{\theta}_k|\mathcal{M}_k)$: parameter priors for all model classes
$\pi(\boldsymbol{y}|\boldsymbol{\theta}_k, \mathcal{M}_k)$: forward model for model class $\mathcal{M}_k$ $\forall$ $k = 1, \ldots, K$
N : number of particles
N_t : number of populations
$\kappa_1, \kappa_2, \ldots, \kappa_T$: thresholds for each population
$K_{p,1}$: parameter perturbation kernel for the first population

1 **for** $t = 0$ to N_t **do**
2   **for** $i = 1$ to N **do**
3   Select candidate model class $\mathcal{M}^* = \mathcal{M}_k$ with probability $P(\mathcal{M}_k)$;
4   **if** $t = 0$ **then**
5   Generate candidate model $\boldsymbol{\theta}^*$ from prior distribution $\pi(\boldsymbol{\theta}|\mathcal{M}^*)$;
6   **else**
7   **repeat**
8   Sample a candidate model $\boldsymbol{\theta}'$ from the previous population's subset $\left\{\boldsymbol{\theta}_{k,t-1}\right\}$ with weights $w_{k,t-1}$;
9   Obtain the perturbed candidate model $\boldsymbol{\theta}^*$ from $K_{p,t}(\boldsymbol{\theta}|\boldsymbol{\theta}')$;
10   **if** $\pi(\boldsymbol{\theta}^*|\mathcal{M}^*) = 0$ **then**
11   Return to step 8 ;
12   **else**
13   Simulate candidate model prediction realization $\mathbf{y}^*$ from $\pi(\boldsymbol{y}|\boldsymbol{\theta}^*, \mathcal{M}^*)$;
14   **end**
15   **until** $\rho(\mathbf{y}^*, \mathbf{d}) \leq \kappa_t$;
16   **end**
17   Set the i^{th} particle as $\mathcal{M}_t^{(i)} = \mathcal{M}^*$, $\boldsymbol{\theta}_t^{(i)} = \boldsymbol{\theta}^*$ with weight $w_t^{(i)}$
18   **end**
19   Normalize the weights $\forall$ $\mathcal{M}_k \in \mathscr{M}$;
20 **end**

FIG. 22: Algorithm 3: Sequential ABC sampler (ABC-SMC) (Toni et al. 2009)

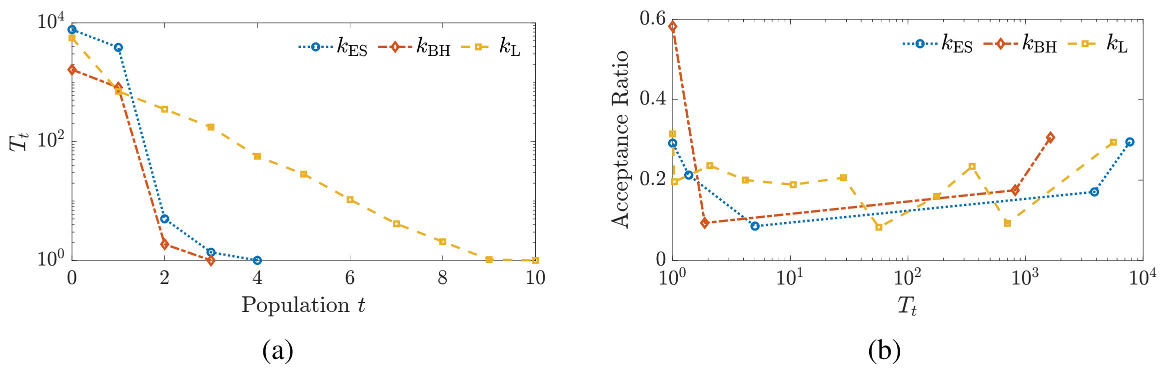

FIG. 23: (a) Temperature values at different populations of the SMC algorithm and (b) corresponding acceptance rates for the base isolated system

Section S1. COMPARISON BETWEEN DIFFERENT FALSIFIERS

Fig. S1 compares the different falsifiers — f_{ES}, f_{EB}, f_{LS} and f_{LB} — in the two-dimensional case of independent standard normal error residuals with a fixed value of the target identification probability. Fig. S1 shows that the likelihood domain falsifiers are more conservative in falsifying models (i.e., retains more models), as compared to the error domain falsifiers. Similarly, FWER control with the Šidák correction is more conservative than FDR control with Benjamini-Hochberg (BH) procedure. Interested readers can refer to (De et al. 2018) for a detailed analysis and comparison of different falsifiers.

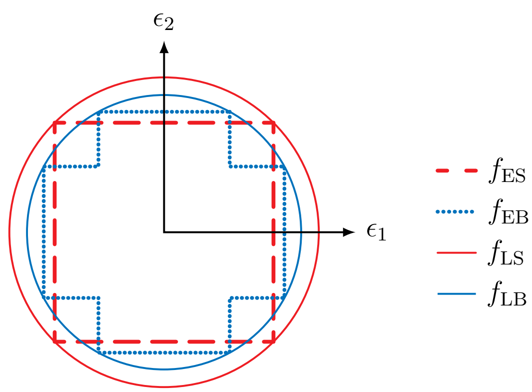

FIG. S1: A comparison of the different falsifiers in two-dimensions for the same target identification probability ϕ. This figure has been adapted from (De et al. 2018)

Section S2. ADDITIONAL RESULTS FOR THE TOY EXAMPLE: EFFECT OF MODEL MISSPECIFICATION

In the toy example, described in Section 5, we had assumed that the falsifiers are based on correct models for the error residuals or, at least, the assumed distributions for the error residuals are similar to the true one. However, that may not be the case and the residual error model may be misspecified. Therefore, in this section, the error residuals are assumed to follow a Laplace distribution, with zero mean and standard deviation σ_ϵ, instead of assuming Gaussian distributions. Fig. S2 shows the approximate posterior pdf obtained using different falsifiers at various levels of target identification probability ϕ when the error residuals are assumed to Laplace distributed. Fig. S3a & b show plots of the mean and COV of the approximate posterior pdf, respectively, as ϕ

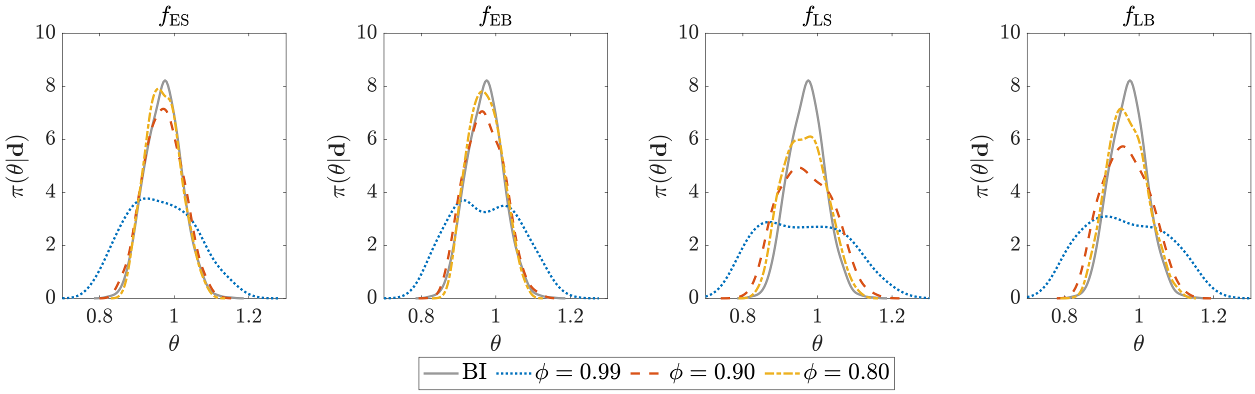

FIG. S2: Approximate posterior pdf obtained using different falsifiers at different levels of ϕ when the probabilistic model for the residual errors is misspecified

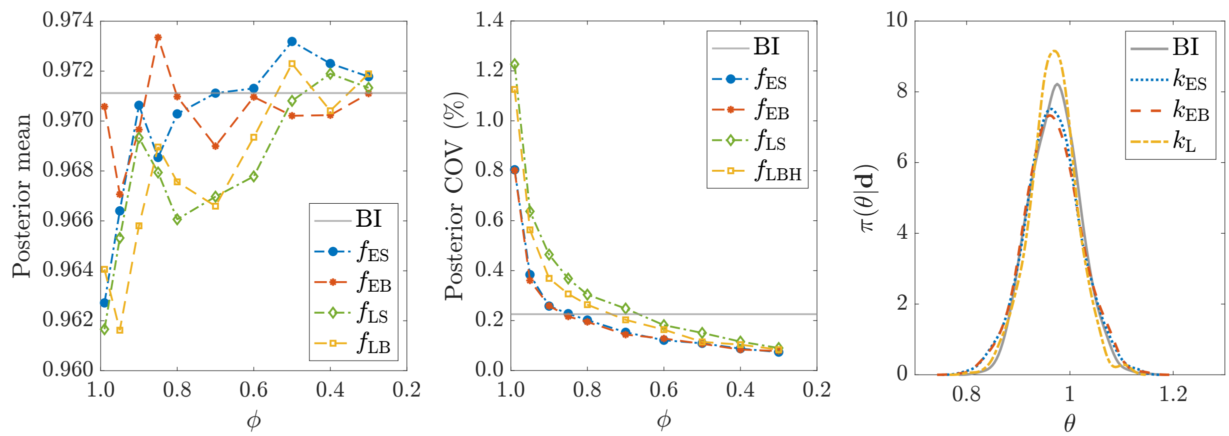

(a) (b) (c)

FIG. S3: (a) Mean and (b) COV of the approximate posterior pdf of θ obtained from model falsified ABC performed using different falsifiers as the target identification probability ϕ is varied, and (c) Approximate posterior pdf obtained using GABC with different kernels when the probabilistic model for the residual errors is misspecified

is decreased. The effect of this misspecfication is more pronounced at the higher values of ϕ. Since the Laplace distribution has heavier tails compared to a Gaussian distribution, more models are unfalsified when the target identification probability is large, resulting in a very poor approximation of the posterior pdf. Again, reducing ϕ can help improve the approximation of the posterior pdf. The performance of model falsified GABC is also affected by the model misspecification. Fig. S3c shows the approximate posterior pdf obtained using model falsified GABC performed using three different kernels. For k_{ES}, k_{EB} and k_{L}, the posterior mean is 0.9670, 0.9672 and 0.9675, and the posterior COV is 0.0029, 0.0030 and 0.0021, respectively. These estimates of θ are more erroneous as compared to those that were obtained when the $\pi_{E_i}(e_i)$ were correctly specified.

Section S3. ADDITIONAL RESULTS FOR THE PARAMETER INFERENCE EXAMPLE OF A CUBIC-QUINTIC OSCILLATOR

Parameter inference using model falsified ABC

The evolution of the posterior mean of the different system parameters through the populations of SMC for different falsifiers is shown in Fig. S4. The run that required the fewest number of populations to reach the target threshold was selected for each falsifier. As the thresholds monotonically decrease between successive populations, the posterior means also move toward the true values, respectively. Fig. S4 offers empirical evidence in support of the consistency of model falsified ABC. The detailed summary statistics of the approximate posterior distributions obtained using model falsified ABC with different model falsifiers is given in Table S1.

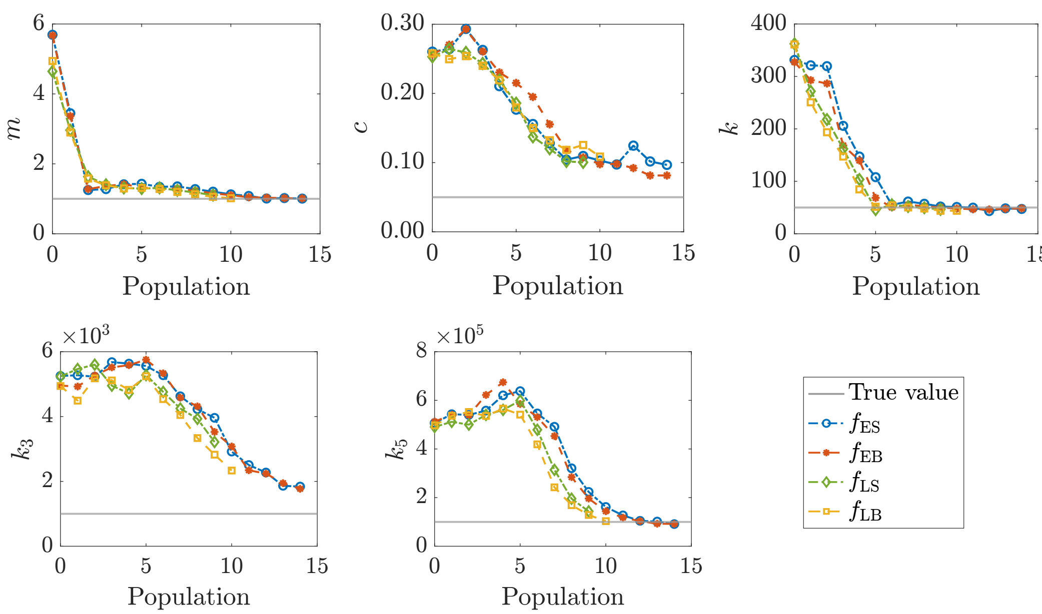

FIG. S4: Evolution of the posterior mean of the various parameters of the cubic-quintic system through the populations of the SMC algorithm. The the true values of the parameters also shown for reference

TABLE S1: Summary of the posterior distribution for the parameters of the cubic-quintic system obtained using model falsified ABC with different model falsifiers. The reported estimates are averages across 10 independent runs

Parameter	Falsifier	Summary of the posterior distribution			Relative error
		Mean	COV	$[5^{th}, 95^{th}]$ percentile	
m	f_{ES}	1.011	0.073	[0.884, 1.123]	0.012
	f_{EB}	1.012	0.067	[0.891, 1.101]	0.014
	f_{LS}	1.039	0.102	[0.848, 1.175]	0.039
	f_{LB}	1.006	0.087	[0.857, 1.160]	0.009
c	f_{ES}	0.091	0.572	[0.018, 0.184]	0.819
	f_{EB}	0.081	0.583	[0.016, 0.167]	0.612
	f_{LS}	0.110	0.654	[0.017, 0.245]	1.198
	f_{LB}	0.104	0.613	[0.016, 0.216]	1.072
k	f_{ES}	48.980	0.216	[30.220, 65.129]	0.020
	f_{EB}	48.856	0.220	[29.197, 64.771]	0.023
	f_{LS}	44.487	0.352	[15.667, 68.351]	0.110
	f_{LB}	44.724	0.299	[20.348, 65.168]	0.106
k_3	f_{ES}	1.67×10^3	0.607	$[0.26 \times 10^3, 3.59 \times 10^3]$	0.668
	f_{EB}	1.66×10^3	0.577	$[0.32 \times 10^3, 3.42 \times 10^3]$	0.662
	f_{LS}	2.54×10^3	0.628	$[0.35 \times 10^3, 5.47 \times 10^3]$	1.535
	f_{LB}	2.11×10^3	0.602	$[0.31 \times 10^3, 4.40 \times 10^3]$	1.113
k_5	f_{ES}	0.92×10^5	0.244	$[0.51 \times 10^5, 1.33 \times 10^5]$	0.083
	f_{EB}	0.90×10^5	0.238	$[0.51 \times 10^5, 1.29 \times 10^5]$	0.097
	f_{LS}	1.07×10^5	0.447	$[0.30 \times 10^5, 1.97 \times 10^5]$	0.081
	f_{LB}	0.92×10^5	0.412	$[0.33 \times 10^5, 1.56 \times 10^5]$	0.082

Parameter inference using model falsified GABC

The detailed summary statistics of the approximate posterior distributions obtained using model falsified GABC with different kernels is given in Table S2.

Section S4. ADDITIONAL RESULTS FOR THE MODEL SELECTION EXAMPLE OF A FOUR DEGREE-OF-FREEDOM BASE ISOLATED STRUCTURE

Model class selection using model falsified ABC

The detailed summary statistics of the parameters of the Bouc-Wen model class obtained using model falsified ABC with different falsifiers is given in Table S3. The corresponding approximate posterior pdfs are shown in Fig. S5.

TABLE S2: Summary of the posterior distribution for the parameters of the cubic-quintic system obtained using model falsified GABC with different kernels and the associated COV given in brackets. The reported estimates for kernel k_{ES} and k_{EB} are averages across 10 independent runs.

Parameter	Kernel	Summary of the posterior distribution			Relative error
		Mean	COV	[5^{th}, 95^{th}] percentile	
m	k_{ES}	0.994	0.065	[0.882, 1.094]	0.006
	k_{EB}	0.997	0.066	[0.884, 1.100]	0.003
	k_{L}	1.022	0.035	[0.964, 1.077]	0.024
c	k_{ES}	0.084	0.541	[0.016, 0.162]	0.676
	k_{EB}	0.083	0.550	[0.016, 0.163]	0.660
	k_{L}	0.041	0.368	[0.015, 0.069]	0.185
k	k_{ES}	48.836	0.196	[32.003, 63.426]	0.023
	k_{EB}	48.446	0.204	[30.637, 63.524]	0.031
	k_{L}	49.016	0.130	[38.654, 59.280]	0.020
k_3	k_{ES}	1.46×10^3	0.594	[0.25×10^3, 3.12×10^3]	0.463
	k_{EB}	1.56×10^3	0.598	[0.26×10^3, 3.29×10^3]	0.565
	k_{L}	1.64×10^3	0.382	[0.59×10^3, 2.58×10^3]	0.644
k_5	k_{ES}	0.90×10^5	0.232	[0.56×10^5, 1.25×10^5]	0.096
	k_{EB}	0.83×10^5	0.249	[0.53×10^5, 1.27×10^5]	0.107
	k_{L}	0.87×10^5	0.1922	[0.61×10^5, 1.15×10^5]	0.133

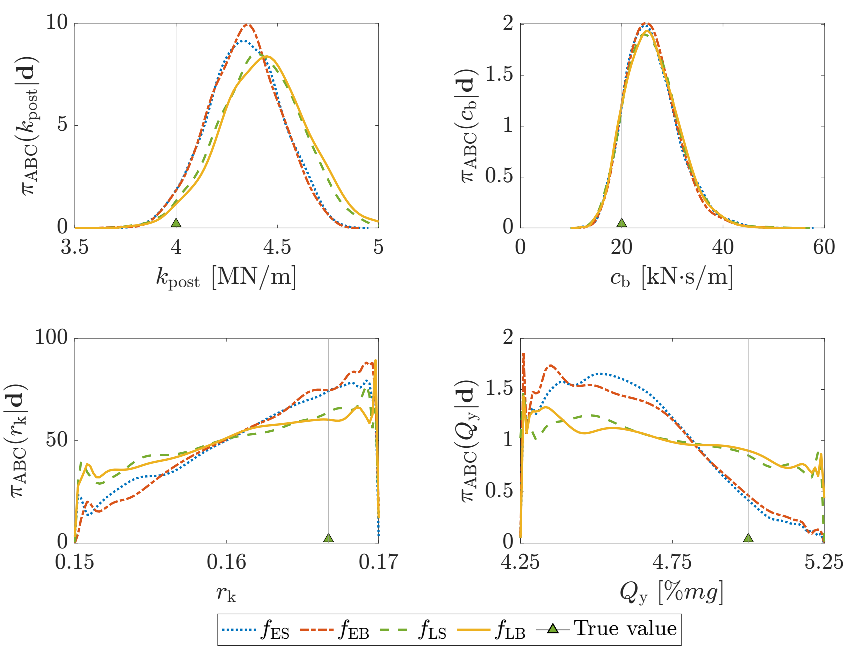

FIG. S5: Approximate posterior pdf of the parameters of the Bouc-Wen model class obtained using model falsified ABC with different falsifiers when $\phi = 0.90$

TABLE S3: Summary of the approximate posterior distribution of the Bouc-Wen model class parameters obtained using model falsified ABC with different model falsifiers when ϕ = 0.90

Parameter	Falsifier	Summary of the posterior distribution			Relative error
		Mean	Std. Dev.	[5th, 95th] percentile	
k_{post} (MN/m)	f_{ES}	4.331	0.181	[4.029, 4.631]	0.082
	f_{EB}	4.327	0.177	[4.026, 4.616]	0.082
	f_{LS}	4.423	0.210	[4.069, 4.769]	0.106
	f_{LB}	4.402	0.206	[4.052, 4.735]	0.100
c_b (kN·s/m)	f_{ES}	24.939	4.976	[17.592, 34.212]	0.247
	f_{EB}	24.911	4.976	[17.883, 33.377]	0.246
	f_{LS}	25.015	5.093	[17.460, 33.863]	0.251
	f_{LB}	25.008	5.054	[17.673, 33.798]	0.250
r_k	f_{ES}	0.1623	0.005	[0.1526, 0.1693]	0.026
	f_{EB}	0.1627	0.005	[0.1531, 0.1694]	0.024
	f_{LS}	0.1613	0.006	[0.1516, 0.1692]	0.032
	f_{LB}	0.1613	0.006	[0.1515, 0.1693]	0.032
Q_y (%mg)	f_{ES}	4.603	0.218	[4.290, 5.001]	0.079
	f_{EB}	4.605	0.227	[4.290, 5.025]	0.079
	f_{LS}	4.700	0.279	[4.289, 5.178]	0.060
	f_{LB}	4.703	0.282	[4.292, 5.178]	0.059

Model class selection using model falsified GABC

The detailed summary statistics of the parameters of the Bouc-Wen model class obtained using model falsified GABC with different kernels is provided in Table S4. The corresponding approximate posterior pdfs are shown in Fig. S6. Figs. S7a and S7b show the approximate posterior predicted mean absolute base acceleration obtained using model falsified GABC with different kernels under the El Centro and Ridgecrest earthquake excitations, respectively.

Section S5. ADDITIONAL RESULTS FOR MODEL FALSIFIER BASED KERNEL REGRESSION

The Nadaraya-Watson estimates for the parameters of the four degree-of-freedom base isolated structure and their relative errors are provided in Table S5. Figs. S8a and S8b show the Nadaraya-Watson estimate for the base absolute acceleration of the four degree-of-freedom base isolated structure under the El Centro and Ridgecrest earthquake excitations, respectively.

TABLE S4: Parameter estimates of the base isolated structure using the GABC approach with different kernels

Parameter	Kernel	Summary of the posterior distribution			Relative error
		Mean	Std. Dev.	[5^{th}, 95^{th}] percentile	
k_{post} (MN/m)	k_{ES}	4.241	0.152	[3.995, 4.502]	0.060
	k_B	4.281	0.172	[3.999, 4.558]	0.070
	k_L	3.986	0.061	[3.878, 4.075]	0.004
c_b (kN·s/m)	k_{ES}	24.621	5.096	[17.061, 33.566]	0.231
	k_B	24.970	4.885	[17.710, 33.992]	0.249
	k_L	25.058	4.781	[17.933, 33.172]	0.253
r_k	k_{ES}	0.1641	0.004	[0.1554, 0.1696]	0.016
	k_B	0.1635	0.005	[0.1541, 0.1695]	0.019
	k_L	0.1661	0.002	[0.1618, 0.1696]	0.004
Q_y (%mg)	k_{ES}	4.704	0.196	[4.380, 5.0270]	0.059
	k_B	4.649	0.219	[4.317, 5.052]	0.070
	k_L	5.034	0.042	[4.967, 5.106]	0.007

TABLE S5: Nadaraya-Watson estimates of the parameters of the base isolated structure obtained using different kernels

Parameter	Kernel	Estimate	Relative Error
k_{post} (MN/m)	k_{ES}	4.382	0.096
	k_{EB}	4.315	0.078
	k_L	4.497	0.124
c_b (kN·s/m)	k_{ES}	24.795	0.239
	k_{EB}	24.963	0.248
	k_L	24.886	0.244
r_k	k_{ES}	0.1608	0.035
	k_{EB}	0.1625	0.025
	k_L	0.1599	0.041
Q_y (%mg)	k_{ES}	4.573	0.085
	k_{EB}	4.617	0.077
	k_L	4.772	0.046

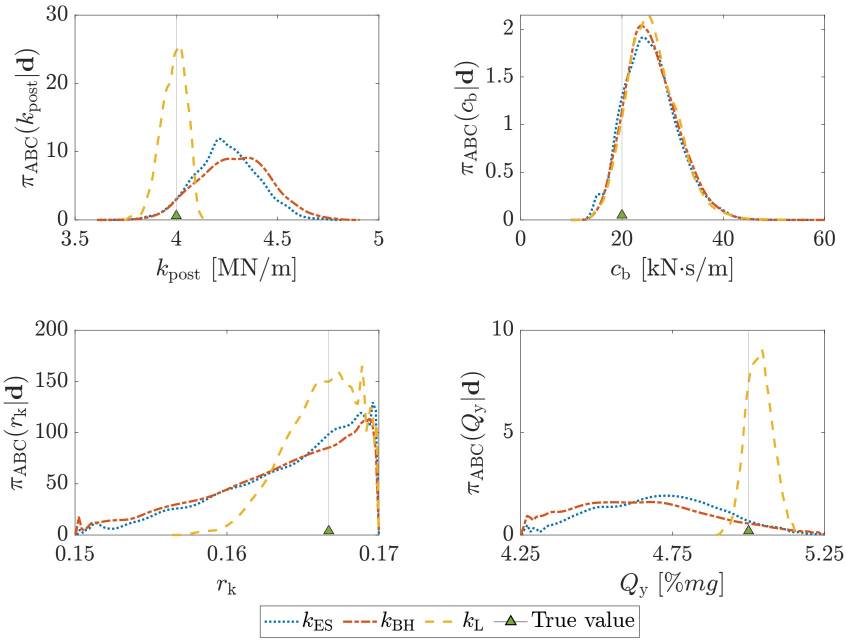

FIG. S6: Approximate posterior pdf of the parameters of the base isolated structure obtained using model falsified GABC with different kernels

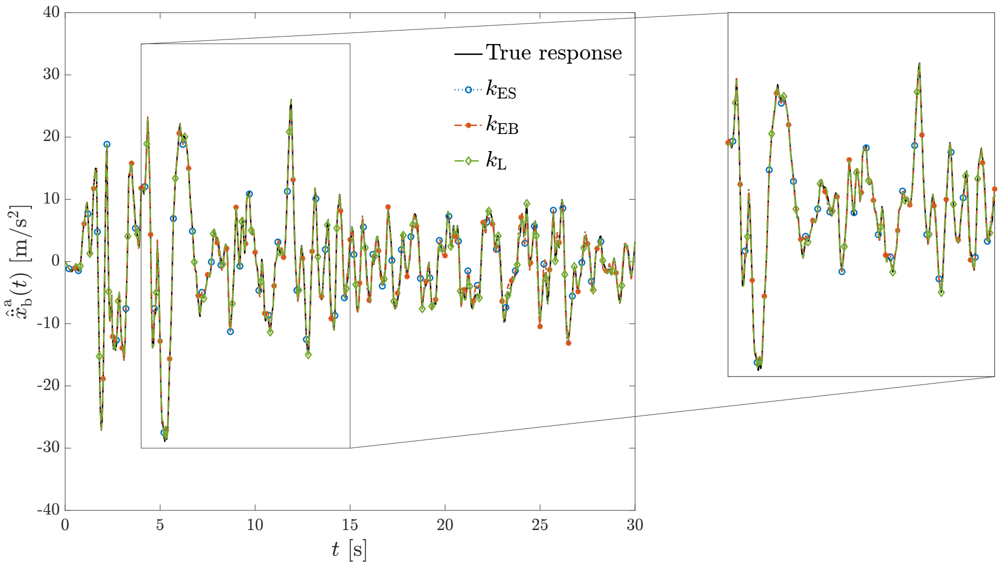

(a) El Centro earthquake excitation

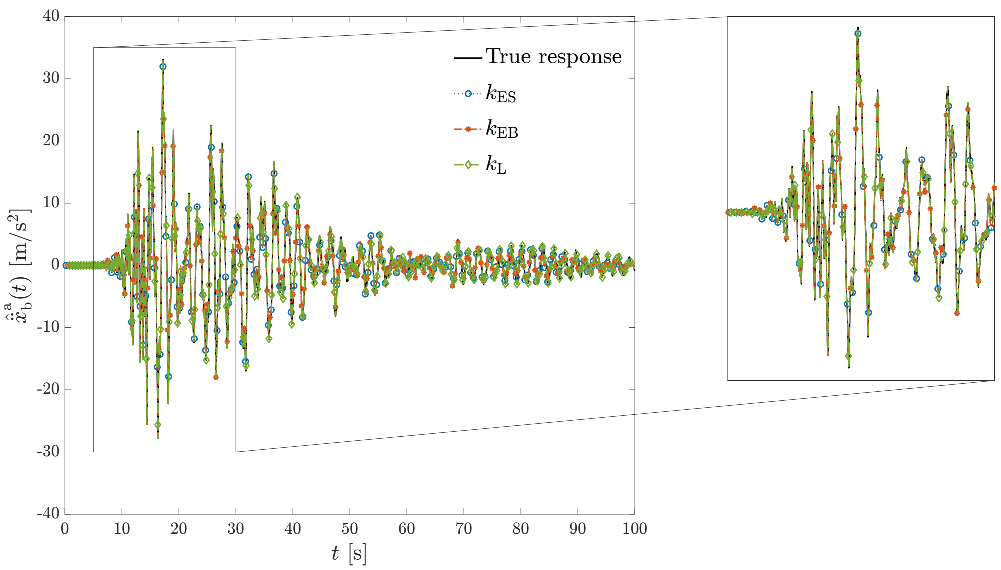

(b) Ridgecrest earthquake excitation

FIG. S7: Approximate posterior predicted mean base absolute acceleration of the base isolated structure under different ground motion excitations from model falsified GABC with different kernels. The measurements are recorded when the structure is excited by the El Centro earthquake excitation

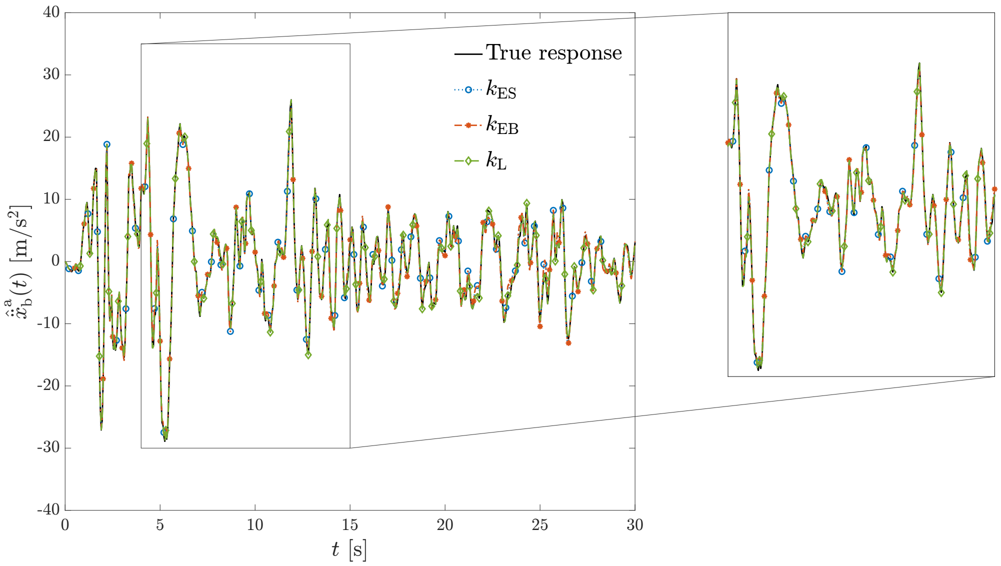

(a) El Centro earthquake excitation

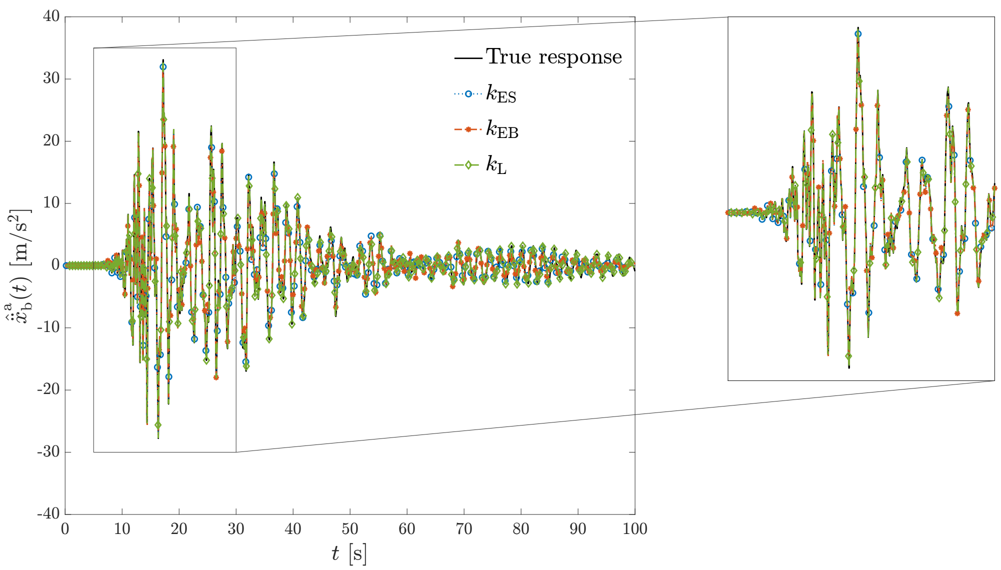

(b) Ridgecrest earthquake excitation

FIG. S8: Nadaraya-Watson estimator for the base absolute acceleration of the base isolated structure under different ground motion excitations computed using different kernels. The measurements are recorded when the structure is excited by the El Centro earthquake excitation

REFERENCES

De, S., Brewick, P. T., Johnson, E. A., and Wojtkiewicz, S. F. (2018). "Investigation of model falsification using error and likelihood bounds with application to a structural system." *Journal of Engineering Mechanics*, 144(9), 04018078. https://doi.org/10.1061/(ASCE)EM.1943-7889.0001440.